Dynamic characteristics and load-sharing performance of concentric face gear split-torque transmission systems with time-varying mesh stiffness, flexible supports and deformable shafts

Jianxiong Dong · Qibo Wang · Jinyuan Tang · Zehua Hu · Xiaoqian Li

Abstract The concentric face gear split-torque transmission system is a new gear mechanism which integrates the advantages of face gears, split-torque transmissions and concentric transmissions. The power transmission through multiple branches improves the systematic load capacity. However, the uniformity of load sharing between branches seriously restricts the service life of the entire system. According to the Newton theorem, a lumped parameter model coupled with the vibrations of the gear with six degrees of freedom, the torsion of input shafts, the meshing of gear pairs, and the bearing supporting is established. Gear backlash, meshing damping, support stiffness, time-varying mesh stiffness, and modified transmission errors are considered in this dynamic model. The discrete solution of dynamic equations is obtained by using the numerical integral method of Runge–Kutta. Natural characteristics and the performance of dynamic load sharing are investigated. Furthermore, the effects of the factors including torsional stiffness, gear backlash and time-varying mesh stiffness on dynamic load sharing are explored. The results indicate that the above-mentioned factors greatly affect the performance of dynamic load sharing, and the phenomenon of tooth disengagement is observed.

Keywords Face gear · Split-torque transmission · Concentric transmission · Lumped parameter model · Dynamic load sharing

J. Dong · Q. Wang (✉) · J. Tang · Z. Hu · X. Li
Light Alloy Research Institute, Central South University, Changsha 410083, China
e-mail: 15116339470@163.com

J. Dong
e-mail: jxdongcsu@163.com

J. Dong
College of Mechanical and Electrical Engineering, Central South University, Changsha 410083, China

Q. Wang · J. Tang · Z. Hu · X. Li
State Key Laboratory of High-Performance Complex Manufacturing, Central South University, Changsha 410083, China

1 Introduction

The face gear transmission has the properties of high speed, heavy load and relatively light weight [1, 2]. In a split-torque transmission, the totally transmitted power can be expanded by the form of multiple transmission branches based on the minimum number of gears [3, 4]. The layout of concentric transmissions is to overlap the gears as coaxial as possible in limited space to reduce the overall size [5, 6]. The advantages of these three aspects are concentrated in a concentric face gear split-torque transmission system (CFGSTTS). Thus, the CFGSTTS has the characteristics of high speed, heavy load, high power density, which has laid a foundation for its application in

aviation transmissions and other fields. As for the multi-branch gear transmission system, failures usually occur earlier in heavy load branches if loads are unevenly shared [4]. Therefore, the evenness of load sharing between branches, especially the dynamic one, is an important limitation to the service life of a gear transmission system.

In the previous work of authors [5, 6], the assembly conditions, time-varying mesh stiffness, transmission error (TE) excitations, simulation modelling, and static load sharing of CFGSTTS have been studied. The highlight of this paper is to analyze the characteristics of dynamic load sharing in CFGSTTS.

1.1 Face gears

In view of the promising prospects and the successful application of face gears in the main reduction system of helicopters in North America, some western European countries called face gears as "the hope of the rotor transmission in twenty-first century". Subsequently, the research about face gears has quickly become a hot topic. Litvin et al. [7–9] systematically probed into the technologies of face gears, including the tooth surface design, tooth modifications, grinding, tooth contact analysis, and the static simulation based on finite element analysis, and they accomplished a related monograph [10]. Zhou et al. [11] established a new method to explicitly calculate the enveloping surface of face gears according to the geometric characteristics of the shaper tooth surface. In this way, the problem of solving nonlinear meshing equations can be avoided. Zschippang et al. [12] elaborated the generation of face gears simultaneously companying with helix angles, shaft angles and axis offsets based on the simulation of enveloping process of face gears. Further, they carried out the tooth contact analysis of face gears. Liu et al. [13] presented a new gear transmission that consist of a planar noncircular gear and an undulating face gear for transmitting varying angular velocities. As they mentioned, this kind of face gears can achieve non-uniform transmission ratios. Shen et al. [14] proposed an optimization methodology to generate the tooth surface of face gears with the method of longitudinal ease-off topography on a multi-axis CNC machine, and this methodology was validated to be suitable for the error correction of tooth flanks. Litvin and Handschuh et al. [1, 15] tested the face gear transmission under the conditions of high speed and heavy load, and the feasibility of application was demonstrated after millions of rotation cycles.

1.2 Dynamics of face gear transmissions

In the aspect of face gear dynamics, the researches mainly focused on the single pair of face gear drive, while few studies on the face gear transmission system were carried out. Hu et al. [16, 17] explored the dynamics of the face gear system that coupled with translation-rotation vibrations by adopting a lumped parameter model (LPM) with fourteen degrees of freedom (DOF), and observed the jump phenomenon, periodic windows, doubling-periodic bifurcations, and chaotic behaviors of the system. Moreover, they researched the effect of mesh stiffness on the dynamic response of the face gear transmission with backlash nonlinearities, and pointed out that the dynamic contact force changed obviously with the forms of mesh stiffness differing. Lin et al. [18, 19] analyzed the dynamic efficiency and dynamic response of an orthogonal face gear system with the impact of meshing frequencies. They summarized that different meshing frequencies led to different dynamic responses, such as chaotic responses, single-cycle responses and multi-cycle responses. Li et al. [20, 21] investigated the dynamic behavior of the face gear with root cracks and constructed an active control solution of face gear webs. Chen et al. [22] analyzed nonlinear jumps, chaotic motions, period doubling bifurcations, and multiple stable solutions of the face gear drive with profile modifications by employing a 6-DOF model concerning gear backlash, time-varying mesh stiffness and moment arms. With the consideration of time-varying instantaneous centers, Liu et al. [23] provided a dynamic model coupled with torsion, bending and translation for a new type of noncircular face gear systems, and presented performance improvement methods to calculate the multi-frequency components in dynamic responses. Zhu et al. [24] analyzed the nonlinear dynamics of the face gear drive system with multi-stage engagements by using a piecewise torsion-bending-translation model. Hu et al. [25, 26] applied a coupled dynamic model to study the kinematics and vibration characteristics of the multi-stage planetary transmission with face gears.

1.3 Load sharing of split-torque transmissions

In a split-torque transmission system, power is transmitted through multiple branches to expand the load capacity of the system without weakening strength of any branch. Theoretically, the transmitted power is evenly shared by parallel branches. Because of inevitable backlash and errors in manufacturing and assembly, the power would be unevenly shared among multiple branches.

According to whether there is a concentric structure, split-torque transmissions can be divided into two categories, namely non-concentric ones and concentric ones. The former is applied earlier and is not the mainstream anymore. White [3] described a split-torque transmission that was composed of double-helical pinions and applied in double-input helicopter transmission systems, and reported the advantages of extremely low height and low power loss in this gear system. Krantz et al. [4] conducted experiments to study tolerances and clocking angles to adjust the load sharing in a split-torque transmission with spur pinions.

The planetary gear is one of the most common types of concentric split-torque transmission systems. Singh et al. [27–29] applied a systematic model of finite element analysis to study the load sharing performance of planetary gears. And they experimentally and theoretically studied the key factors that affect the gear stress and load sharing in planetary transmissions. Montestruc [30, 31] numerically calculated the load sharing coefficient (LSC) between planets in a planetary gear drive with the variables of planet number and spring constant, and he also studied the influence of planet pin stiffness on load sharing. Iglesias et al. [32] researched the quasi-static load sharing of the planetary transmission with the effect of radial positioning errors of planets. According to the formation of interference zones and high stress zones, Li et al. [33] predicted the reliability of planetary gear trains under the condition of partial loads. Mo et al. [34] analytically investigated the dynamic load sharing of herringbone planetary gears, and studied the influence mechanism of the flexible support on load sharing characteristics.

Currently, there is little research on CFGSTTS, especially on the dynamics. Dong et al. [5, 6] investigated the assembly conditions, static power flow directions and load sharing of CFGSTTS, and

proposed a semi-analytical method to compute the mesh stiffness of the gear pairs in this system. Mo et al. [35] established a LPM which considered the translational and torsional vibrations of gears for CFGSTTS. Unfortunately, the dynamic models in current researches on CFGSTTS did not mention such important factors as the torsional flexibility of shafts, the gear backlash and the time-varying mesh stiffness. The dynamic load sharing of CFGSTTS was also not comprehensively analyzed by dissecting power flow directions, and the DOFs of gear deformation were incompletely considered. In conclusion, current researches either studied the static load sharing of CFGSTTS or ideally analyzed the dynamic load sharing between input gears, rather than delving into other more important issues, such as the dynamic load sharing between face gears.

In this paper, a LPM which simultaneously considers gear backlash, meshing damping, TE excitations, torsional stiffness, support stiffness, and time-varying mesh stiffness for CFGSTTS is proposed. Firstly, the TE formula is modified according to the characteristics of face gear drives. The expressions of time-varying mesh stiffness and TE excitations in the dynamic model are introduced. Secondly, the natural characteristics of CFGSTTS, such as critical speeds and modals, are explored based on the established dynamic model. The dynamic load sharing among multiple branches is researched according to the power flow direction, and the speed-sweep response is involved. Then, the proposed model is validated by comparing the results of the proposed model and the ADAMS simulation. Finally, the effects of system parameters including gear backlash, torsional stiffness, and time-varying mesh stiffness on dynamic load sharing performance are investigated.

2 Modeling

2.1 Structure

A CFGSTTS is composed of two face gears and several pinions. The two face gears are oppositely assembled, and the pinions are distributed around the circumference of the face gears. The tooth surface parameters of the two face gears are identical, so are the pinions. The structural characteristics of CFGSTTS can meet the requirements of multi-input

and multi-output for transmission mechanisms such as the gear systems in helicopters. Moreover, the structure of CFGSTTS is space-saving because of the concentricity. The gears with same tooth surface parameters have differences in gear structure, which is determined by their different roles in the system. During the transmission process, all pinions rotate in the same direction around their respective axes, but two face gears rotate in opposite directions.

Actually, a CFGSTTS can be composed of different numbers of pinions as long as the conditions of assembly and non-interference [5] are met. As demonstrated in Fig. 1, the CFGSTTS mentioned in this article contains five pinions. Different to idler gears and tail gear, two input gears are connected to engines via input shafts.

In the CFGSTTS showed in Fig. 1, power is input from left input and right input, and output from upper face gear and tail gear. During the process of power transmitting, there is a problem whether the load sharing between branches is even or not. Before the issue of load sharing is classified and discussed, the power flow direction should be figured out. If the assembly conditions in Ref. [5] are met, the positions of pinions are determined by distribution angles γ_j (j = 1, 2, 3, 4, 5), as illustrated in Fig. 2.

2.2 Physical model

The dynamic responses of CFGSTTS are generated from the torsion of input shafts, the gear meshing, the supporting of bearings, and the translation, bending and torsion of gear bodies. In fact, the whole system is flexible and will deform accordingly. The deformation coordination and coupling relations are very complex, so some assumptions are proposed.
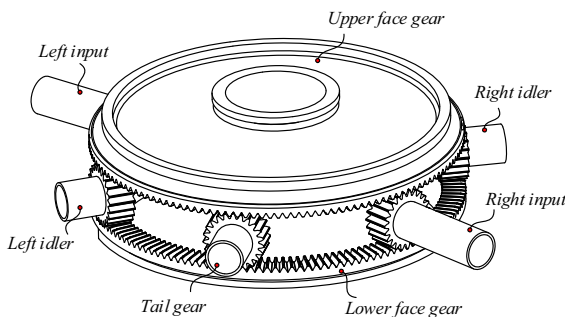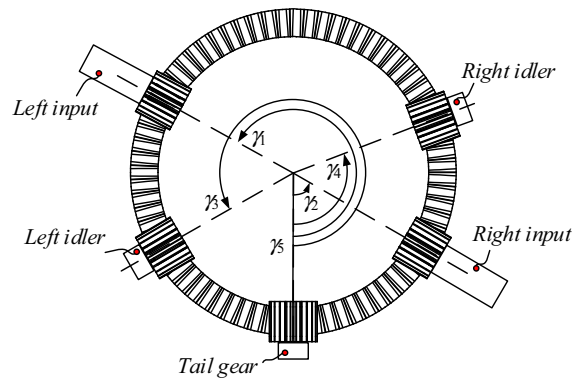

Fig. 1 Three-dimensional model

Fig. 2 Top view

(i) The torsional deformation of input shafts, the meshing deformation of gear pairs, and the supporting deformation of bearings are considered. The hubs of face gears and pinions are assumed to be rigid.

(ii) For different gear pairs, the TE excitation and mesh stiffness are consistent and time-varying, while the meshing damping and backlash are consistent and constant. There may be phase differences in the transmission error (TE) excitation and mesh stiffness between different gear pairs.

(iii) The torsional stiffness of two input shafts is equivalent constant, so are the supporting stiffness of five pinions and the supporting stiffness of two face gears.

As illustrated in Fig. 3, the masses of gears No. 1–7 are M_k (k =1, 2…7), the polar inertia of the gears is J_{kz}, the diameter moments of inertia about x-axis and y-axis are J_{kx} and J_{ky}, respectively, and k_{kx}, k_{ky}, k_{kz} respectively denotes the support stiffness component in each coordinate direction.

For the ten gear pairs that are composed of five pinions and two face gears, e_{ij} (i = 6, 7; j = 1, 2…5) represents the TE excitation, and b_{ij} means the half value of backlash. The meshing damping coefficient is c_{ij}, and the time-varying mesh stiffness is k_{ij}.

The polar inertia of two input shafts is J_{np} (n =1, 2), the torsional stiffness is k_{nt}, and the driving torque is T_n.

Additionally, the symbol T_U is the torque stressed on upper face gear, the symbol T_O denotes the torque stressed on tail gear, and the symbol Z_w (w = p, g) is the tooth number of the pinion and the face gear.
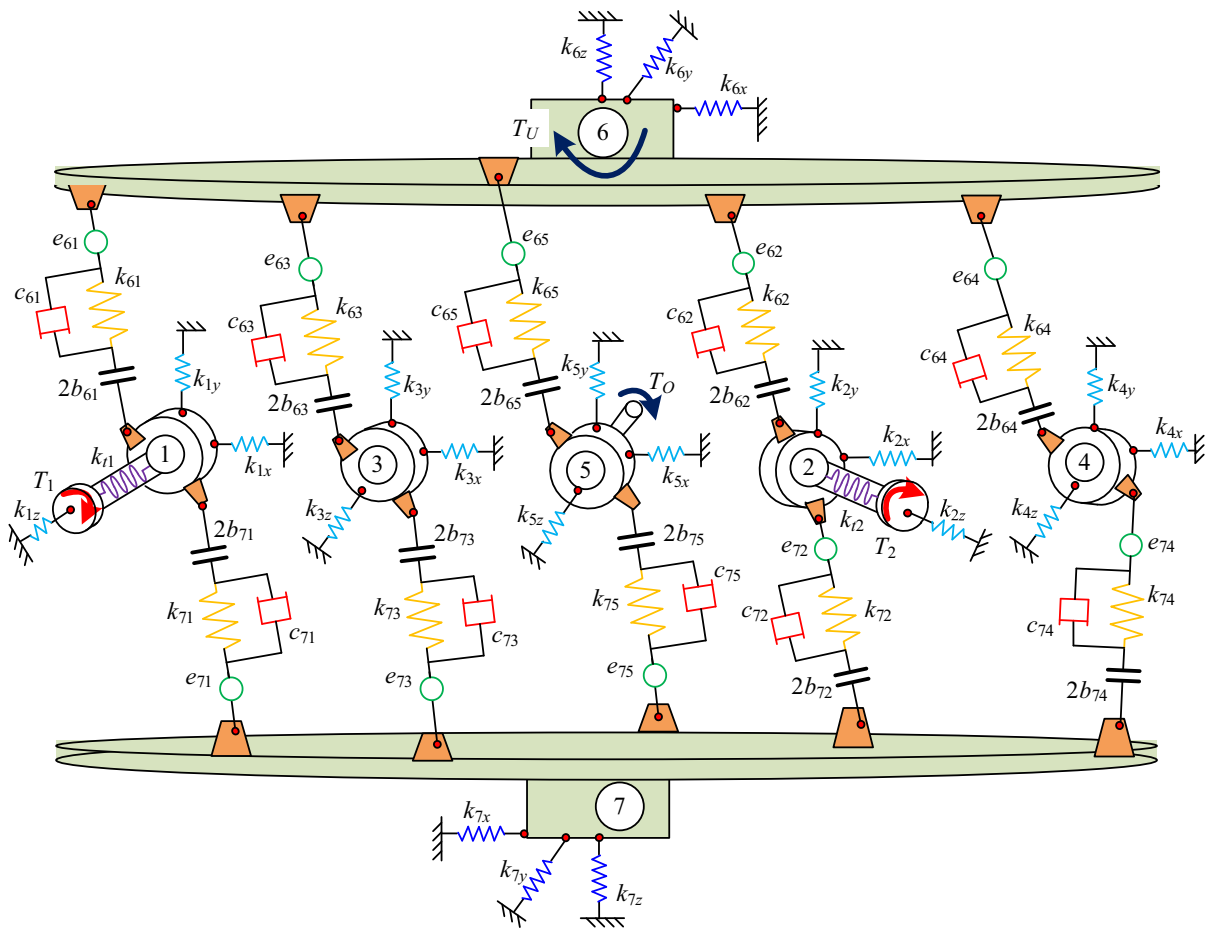
Fig. 3 Physical model

2.3 Excitations

There are many types of external and internal excitations in this dynamic model, as illustrated in Fig. 3. The internal excitations mainly cover the gear backlash, the meshing damping, the support stiffness, the torsional stiffness of input shafts, the time-varying mesh stiffness, and the time-varying TE excitations. While the external excitations are mainly the load torques that act on upper face gear and tail gear. The highlight of this section is the time-varying mesh stiffness and the modified TE of face gear drives.

2.3.1 Time-varying mesh stiffness

The mesh stiffness is one of the main sources resulting in the vibrations of gear systems. In Ref. [6], it has been proved that the mesh stiffness of the gear pairs in

CFGSTTS is time-varying, periodic and load-dependent. The mesh stiffness obtained by the simulation of CFGSTTS cannot be used to solve the dynamic equations, because the stiffness involves the influence of the system structural deformation, however, this influence has been already considered in the dynamic equations. Therefore, the mesh stiffness is figured out by the simulation of single gear pair instead of the simulation of the whole system.

Firstly, the CFGSTTS should be simulated to compute the contact forces of gear pairs in the system, and the average of the contact forces is calculated as the load torque T_m. Then, the single pair of face gear is simulated under the condition of load torque T_m, and the meshing deformation δ can be figured out through the rotation angles θ_w ($w = p$, g) of gears, which is $\delta = r_p * \theta_p - r_g * \theta_g$. Finally, the mesh stiffness can be

calculated as T_m/δ. The details of the finite element simulation of gears are introduced in Ref. [6].

In this dynamic model, the periodic mesh stiffness is converted into the form of Fourier series.

$$k_{ij}(t) = \sum_{\zeta=0}^{\infty} \left[a_\zeta \sin j\omega_m \left(t - \phi_j + \psi_j \right) \right. \\ \left. + b_\zeta \cos j\omega_m \left(t - \phi_j + \psi_j \right) \right] \qquad (1)$$

Here, k_{ij} ($i = 6, 7; j = 1, 2\ldots5$) is the mesh stiffness of gear pairs, and a_ζ and b_ζ are the coefficients of harmonic components. ϕ_j is the phase angle which is related to the distribution angle, and ψ_j is the phase angle related to the face gear position. ω_m is the meshing frequency. In Fig. 2, tail gear is taken as the datum, and the phase angles can be formulated as

$$\phi_j = \frac{Zg\gamma_j}{2\pi} T \\ \psi_j = \begin{cases} 0 & \textit{upper face gear} \\ T/2 & \textit{lower face gear} \end{cases} \qquad (2)$$

where T is the meshing period, and γ_j ($j = 1, 2, \ldots, 5$) is the distribution angle illustrated in Fig. 2.

One of the pinions should be selected as the referential gear at first, and its phase angle is defined as 0. Then, the phase angles of other pinions can be calculated by using Eq. (2).

2.3.2 Modified transmission error of face gears

The TE is defined as the difference between the actual angular position of the driven gear and where it would be if all gears were perfect [36]. Generally, the TE is modelled as a periodic displacement excitation along the meshing line.

In a spur gear drive, both the angular displacements of the driving gear and the driven gear function along the meshing line, as showed in Fig. 4a, and the TE can be expressed as their difference. However, in a face gear drive, the angular displacement of the pinion is tangential along the pitch circle, and the angular displacement of the face gear acts along the peripheral direction, as demonstrated in Fig. 4b.

Actually, the face gear has no meshing line, so the TE of the face gear drive should be tangential along the pitch circle of the pinion. The TE formula of face gear drives should be modified and expressed as

$$\Gamma = r_p\theta_p - r_g\theta_g \cos \alpha \qquad (3)$$

Here, the symbol Γ means the TE, and the symbol α is the pressure angle. r_p and r_g respectively represent the moment arms of the driving gear and the driven gear. The symbols θ_p and θ_g represent the rotational angles of the driving gear and the driven gear, respectively.

Both the definitions of dynamic transmission error (DTE) and unloaded TE of face gear drives are formulated in Eq. (3). Differently, the unloaded TE is an internal excitation, and can be obtained in advance according to the finite element simulation under the condition of a slight load. In the calculation of unloaded TE excitations, the rotation angles θ_p and θ_g can be extracted from the finite element simulation, which is introduced in Ref. [6]. However, the DTE is a response that can only be calculated after the dynamics equations are solved.

Similar to the mesh stiffness, the time-varying unloaded TE is also discretized into the Fourier series in Eq. (1) whose high-order harmonics can be filter out according to specific accuracy. For the same gear pair,

Fig. 4 Schematic diagrams of TEs (**a**) Spur gear drive (**b**) Face gear drive
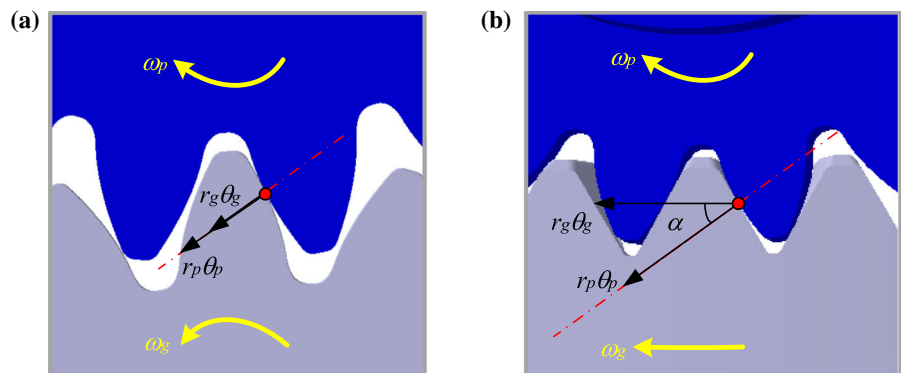
the phase of unloaded TE is consistent with that of the mesh stiffness.

2.4 Dynamic model

Ref. [35] researched the translational vibration and the torsional vibration of CFGSTTS based on a LPM. However, some important factors such as torsional flexibility of shaft, gear backlash and time-varying meshing stiffness are not considered. The dynamic load sharing of the system is not fully analyzed by dissecting the power flow direction, and the deformed DOFs considered are incomplete.

In the dynamic model of CFGSTTS in this paper, each gear has three translational DOFs that are x_k, y_k, z_k ($k = 1, \ldots 7$), and three rotational DOFs that are θ_{kx}, θ_{ky}, θ_{kz}, as demonstrated in Fig. 5. As the torsional deformation of two input shafts is considered, there should be two rotational DOFs which are represented by the symbol θ_{np} ($n = 1, 2$).

Consequently, there are as many as 44 DOFs in this dynamic model, which forms the generalized coordinate system as presented below.

$$\boldsymbol{q} = [x_1, y_1, z_1, \theta_{1x}, \theta_{1y}, \theta_{1z}, x_2, y_2, z_2, \theta_{2x}, \theta_{2y}, \theta_{2z} \\ \ldots, x_7, y_7, z_7, \theta_{7x}, \theta_{7y}, \theta_{7z}, \theta_{1p}, \theta_{2p}]^T \tag{4}$$

According to the definition, the meshing deformation δ of a face gear drive should be reflected as the difference between the DTE and the unloaded TE.

$$\delta = \Gamma - e \tag{5}$$

Here, the symbol Γ denotes the DTE in Eq. (3), and the symbol e is the unloaded TE which is calculated based on the errors of geometric model and gear

backlash. In general, the unloaded TE is much smaller than the DTE, so the meshing deformation is basically equal to the DTE. To demonstrate the relationship between the meshing deformation δ in Eq. (5) and the generalized coordinate related to the DOF in Eq. (4), the intermediate coordinate system S_{ij} (x_{ij}, y_{ij}, z_{ij}) ($i = 6, 7$; $j = 1, 2 \ldots 5$) is set up as Fig. 6.

The transformation matrix between the intermediate coordinate S_{ij} and the generalized coordinate in Eq. (4) is

$$\begin{bmatrix} x_{6j} \\ y_{6j} \\ z_{6j} \end{bmatrix} = \begin{bmatrix} \cos \gamma_j & -\sin \gamma_j & 0 \\ \sin \gamma_j & \cos \gamma_j & 0 \\ 0 & 0 & 1 \end{bmatrix} \begin{bmatrix} x_6 \\ y_6 \\ z_6 \end{bmatrix} \tag{6}$$

$$\begin{bmatrix} x_{7j} \\ y_{7j} \\ z_{7j} \end{bmatrix} = \begin{bmatrix} \cos \gamma_j & \sin \gamma_j & 0 \\ -\sin \gamma_j & \cos \gamma_j & 0 \\ 0 & 0 & 1 \end{bmatrix} \begin{bmatrix} x_7 \\ y_7 \\ z_7 \end{bmatrix} \tag{7}$$

Where γ_j ($j = 1, 2, \ldots, 5$) is the distribution angle illustrated in Fig. 2.

According to Eqs. (3), (5), (6) and (7), the meshing deformation can be expressed by the generalized coordinate in Eq. (4) as

$$\delta 6j = [xj - (\cos \gamma j x6 - \sin \gamma j y6)] \cos \alpha \\ + (yj + z6) \sin \alpha + rp\theta j - rg\theta 6 \cos \alpha - e6j \tag{8}$$

$$\delta 7j = [xj - (\cos \gamma j x7 + \sin \gamma j y7)] \cos \alpha \\ + (yj - z7) \sin \alpha + rp\theta j - rg\theta 7 \cos \alpha - e7j \tag{9}$$

Here, j ($j = 1, 2 \ldots, 5$) represents the pinion number. The unloaded TEs e_{6j} and e_{7j} in Eqs. (5, 8 and 9) should be consistent with the TE excitations in Fig. 3. Besides, the torsional deformation angles ($\delta_{n\theta} = 1, 2$) of the input shafts are
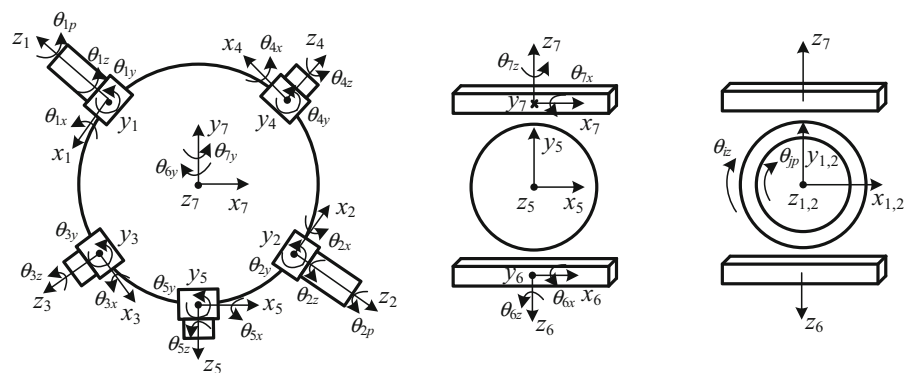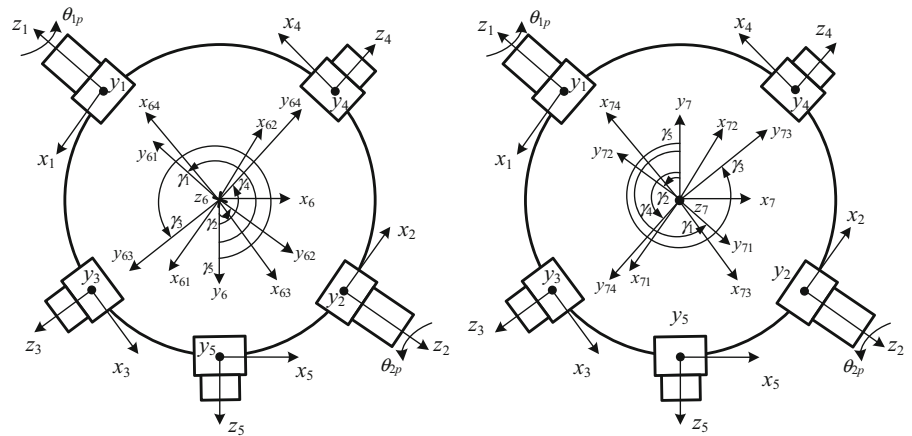

Fig. 5 Generalized coordinate

Fig. 6 Intermediate coordinate

$$\delta n\theta = \theta np - \theta nz \qquad (10)$$

where the symbols θ_{np} and θ_{nz} are the generalized coordinate in Eq. (4).

Because of the existence of gear backlash, the actual meshing deformation δ_{ij} ($_i$ = 6, 7; $_j$ = 1, 2…5) should be replaced by the non-linear displacement function $f(\delta_{ij})$ [36], and can be formulated as

$$f(\delta ij) = \begin{cases} \delta ij - bij & \delta ij \ge bij \\ 0 & |\delta ij| < bij \\ \delta ij + bij & \delta ij \le -bij \end{cases} \qquad (11)$$

Correspondingly, the dynamic contact force F_{ij} [37] of a gear pair can be obtained based on the mesh stiffness k_{ij} and the meshing damping c_{ij}.

$$Fij = \begin{cases} kij(\delta ij - bij) + cij\dot{\delta} ij & \delta ij \ge bij \\ 0 & |\delta ij| < bij \\ kij(\delta ij + bij) - cij\dot{\delta} ij & \delta ij \le -bij \end{cases} \qquad (12)$$

The dynamic equations of the gears numbered 1–7 in Fig. 3 can be established based on force analysis in the generalized coordinate in Eq. (4). In the investigation of the input terminals, the force analysis of an input shaft and an input gear is carried out separately. Each translational and angular DOF of gears respectively corresponds to an equilibrium equation.

The input gear without shaft is not directly driven by input power and achieves dynamic balance under the combined action of contact forces, damping forces, supporting forces and inertia forces. Thus, the dynamic equations of left and right input gears are Eqs. (13 and 14), respectively.

$$\begin{cases} M1\ddot{x}1 + cos\alpha(c61\dot{\delta}61 + c71\dot{\delta}71) + \cos\alpha[k61f(\delta61) + k71f(\delta71)] + k1xx1 = 0 \\ M1\ddot{y}1 + \sin\alpha(c61\dot{\delta}61 + c71\dot{\delta}71) + \sin\alpha[k61f(\delta61) + k71f(\delta71)] + k1yy1 = 0 \\ M1\ddot{z}1 + k1zz1 = 0 \\ J1x\ddot{\theta}1x = 0 \\ J1y\ddot{\theta}1y = 0 \\ J1z\ddot{\theta}1z + rp(c61\dot{\delta}61 + c71\dot{\delta}71) + rp[k61f(\delta61) + k71f(\delta71)] - k1t(\theta1p - \theta1z) = 0 \end{cases} \qquad (13)$$

$$\begin{cases} M2\ddot{x}2 + cos\alpha(c62\dot{\delta}62 + c72\dot{\delta}72) + \cos\alpha[k62f(\delta62) + k72f(\delta72)] + k2xx2 = 0 \\ M2\ddot{y}2 + \sin\alpha(c62\dot{\delta}62 + c72\dot{\delta}72) + \sin\alpha[k62f(\delta62) + k72f(\delta72)] + k2yy2 = 0 \\ M2\ddot{z}2 + k2zz2 = 0 \\ J2x\ddot{\theta}2x = 0 \\ J2y\ddot{\theta}2y = 0 \\ J2z\ddot{\theta}2z + rp(c62\dot{\delta}62 + c72\dot{\delta}72) + rp[k62f(\delta62) + k72f(\delta72)] - k2t(\theta2p - \theta2z) = 0 \end{cases} \qquad (14)$$

In Eqs. (13 and 14), the lateral rotation of the two input gears is not affected by the moments, so the bending vibrations are only affected by the inertia forces.

Similarly, the dynamic equations of left idler and right idler can be obtained, and respectively expressed by Eqs. (15 and 16). However, the tail gear is stressed by a small load torque, and its dynamic equation is Eq. (17).

The axial vibrations of two face gears are affected by contact forces and damping forces, which is different from five pinion gears. Moreover, upper face gear bears a large load torque because it outputs the main power of the system. Thus, the dynamic equations of two face gears are presented as Eqs. (18 and 19), respectively.

$$
\begin{cases}
M3\ddot{x}3 + cos\alpha(c63\dot{\delta}63 + c73\dot{\delta}73) + cos\alpha[k63f(\delta63)+k73f(\delta73)] + k3xx3=0 \\
M3\ddot{y}3 + \sin\alpha(c63\dot{\delta}63 + c73\dot{\delta}73) + sin\alpha[k63f(\delta63)+k73f(\delta73)] + k3yy3=0 \\
\quad M3\ddot{z}3 + k3zz3= 0 \\
\quad J3x\ddot{\theta}3x= 0 \\
\quad J3y\ddot{\theta}3y= 0 \\
\quad J3z\ddot{\theta}3z + rp(c63\dot{\delta}63 + c73\dot{\delta}73)+rp[k63f(\delta63)+k73f(\delta73)]=0
\end{cases}
\tag{15}
$$

$$
\begin{cases}
M4\ddot{x}4 + cos\alpha(c64\dot{\delta}64 + c74\dot{\delta}74) + cos\alpha[k64f(\delta64)+k74f(\delta74)] + k4xx4=0 \\
M4\ddot{y}4 + \sin\alpha(c64\dot{\delta}64 + c74\dot{\delta}74) + sin\alpha[k64f(\delta64)+k74f(\delta74)] + k4yy4=0 \\
\quad M4\ddot{z}4 + k4zz4= 0 \\
\quad J4x\ddot{\theta}4x= 0 \\
\quad J4y\ddot{\theta}4y= 0 \\
\quad J4z\ddot{\theta}4z + rp(c64\dot{\delta}64 + c74\dot{\delta}74)+rp[k64f(\delta64)+k74f(\delta74)]=0
\end{cases}
\tag{16}
$$

$$
\begin{cases}
M5\ddot{x}5 + cos\alpha(c65\dot{\delta}65 + c75\dot{\delta}75) + cos\alpha[k65f(\delta65)+k75f(\delta75)] + k5xx5=0 \\
M5\ddot{y}5 + \sin\alpha(c65\dot{\delta}65 + c75\dot{\delta}75) + sin\alpha[k65f(\delta65)+k75f(\delta75)] + k5yy5=0 \\
\quad M5\ddot{z}5 + k5zz5= 0 \\
\quad J5x\ddot{\theta}5x= 0 \\
\quad J5y\ddot{\theta}5y= 0 \\
\quad J5z\ddot{\theta}5z+rp(c65\dot{\delta}65 + c75\dot{\delta}75) + rp[k65f(\delta65)+k75f(\delta75)]= - TO
\end{cases}
\tag{17}
$$

$$
\left\{
\begin{array}{l}
M6\ddot{x}6 - \cos\alpha(c61\dot{\delta}61\cos\gamma1 + c62\dot{\delta}62\cos\gamma2 + c63\dot{\delta}63\cos\gamma3 + c64\dot{\delta}64\cos\gamma4 + c65\dot{\delta}65) - \\
\cos\alpha[\cos\gamma1k61f(\delta61) + \cos\gamma2k62f(\delta62) + \cos\gamma3k63f(\delta63) + \cos\gamma4k64f(\delta64) + k65f(\delta65)] + k6xx6 = 0 \\
M6\ddot{y}6 + (c61\dot{\delta}61\sin\gamma1 + c62\dot{\delta}62\sin\gamma2 + c63\dot{\delta}63\sin\gamma3 + c64\dot{\delta}64\sin\gamma4 + c65\dot{\delta}65)\cos\alpha + \\
\cos\alpha[\sin\gamma1k61f(\delta61) + \sin\gamma2k62f(\delta62) + \sin\gamma3k63f(\delta63) + \sin\gamma4k64f(\delta64)] + k6yy6 = 0 \\
M6\ddot{z}6 + \sin\alpha(c61\dot{\delta}61 + c62\dot{\delta}62 + c63\dot{\delta}63 + c64\dot{\delta}64 + c65\dot{\delta}65) + \\
\sin\alpha[k61f(\delta61) + k62f(\delta62) + k63f(\delta63) + k64f(\delta64) + k65f(\delta65)] + k6zz6 = 0 \\
J6x\ddot{\theta}6x = 0 \\
J6y\ddot{\theta}6y = 0 \\
J6z\ddot{\theta}6z - rg(c61\dot{\delta}61 + c62\dot{\delta}62 + c63\dot{\delta}63 + c64\dot{\delta}64 + c65\dot{\delta}65)\cos\alpha - \\
rg\cos\alpha[k61f(\delta61) + k62f(\delta62) + k63f(\delta63) + k64f(\delta64) + k65f(\delta65)] = -TU
\end{array}
\right.
\tag{18}
$$

$$
\left\{
\begin{array}{l}
M7\ddot{x}7 - \cos\alpha(c71\dot{\delta}71\cos\gamma1 + c72\dot{\delta}72\cos\gamma2 + c73\dot{\delta}73\cos\gamma3 + c74\dot{\delta}74\cos\gamma4 + c75\dot{\delta}75) - \\
\cos\alpha[\cos\gamma1k71f(\delta71) + \cos\gamma2k72f(\delta72) + \cos\gamma3k73f(\delta73) + \cos\gamma4k74f(\delta74) + k75f(\delta75)] + k7xx7 = 0 \\
M7\ddot{y}7 - \cos\alpha(c71\dot{\delta}71\sin\gamma1 + c72\dot{\delta}72\sin\gamma2 + c73\dot{\delta}73\sin\gamma3 + c74\dot{\delta}74\sin\gamma4 + c75\dot{\delta}75) - \\
\cos\alpha[\sin\gamma1k71f(\delta71) + \sin\gamma2k72f(\delta72) + \sin\gamma3k73f(\delta73) + \sin\gamma4k74f(\delta74)] + k7yy7 = 0 \\
M7\ddot{z}7 - \sin\alpha(c71\dot{\delta}71 + c72\dot{\delta}72 + c73\dot{\delta}73 + c74\dot{\delta}74 + c75\dot{\delta}75) - \\
\sin\alpha[k71f(\delta71) + k72f(\delta72) + k73f(\delta73) + k74f(\delta74) + k75f(\delta75)] + k7zz7 = 0 \\
J7x\ddot{\theta}7x = 0 \\
J7y\ddot{\theta}7y = 0 \\
J7z\ddot{\theta}7z - rg(c71\dot{\delta}71 + c72\dot{\delta}72 + c73\dot{\delta}73 + c74\dot{\delta}74 + c75\dot{\delta}75)\cos\alpha - \\
rg\cos\alpha[k71f(\delta71) + k72f(\delta72) + k73f(\delta73) + k74f(\delta74) + k75f(\delta75)] = 0
\end{array}
\right.
\tag{19}
$$

Two input shafts tend to balance under the combined action of the driving torques, the inertial forces and the reaction torques from input gears. Their dynamic equations are expressed by Eq. (20).

$$
\left\{
\begin{array}{l}
J1p\ddot{\theta}1p + k1t(\theta1p - \theta1z) = T1 \\
J2p\ddot{\theta}2p + k2t(\theta2p - \theta2z) = T2
\end{array}
\right.
\tag{20}
$$

After the Eqs. (13–20) are jointly solved, the dynamic response of each DOF can be obtained. Then, the dynamic contact force of each gear pair can be achieved, and the load sharing can be analyzed.

Generally, the LSC [5] is applied to measure the uniformity of load sharing in a split-torque transmission system, which is defined as

$$
\varepsilon = \frac{NMax(rpF\varsigma)}{\sum_{\varsigma=1}^{N} rpF\varsigma}
\tag{21}
$$

where N is the path number of power transmission, and F_ζ is the contact force of a gear pair.

3 Numerical examples

The geometric parameters and the structural parameters of CFGSTTS in this paper are presented in Table 1. Based on these parameters, the geometric model of CFGSTTS can be established.

As demonstrated in Table 2, the mass and inertia of each gear can be measured directly in the CATIA software based on the geometric model. Besides, the support stiffness can be calculated in KissSoft software according to the working condition presented in Table 3. Referring to current experience and Ref. [16], the backlash value of each gear pair is temporarily set at 20 um.

Table 1 Geometric parameters of CFGSTTS

Parameters	Pinion	Face gear
Modulus m (mm)	3.75	
Pressure angle α (°)	25	
Shaft angle η (°)	90	
Helical angle β (°)	0	
Distribution angle $\gamma_1, \gamma_2, \gamma_3, \gamma_4, \gamma_5$ (°)	245.455/114.545/303.375/56.643/0	
Tooth number Z_p/Z_g	23	143
Tooth width B (mm)	40	35 (R280/r245)

Table 2 Dynamic parameters of CFGSTTS

Parameters	Values
Material density ρ (kg.m^{-3})	7840
Mass of pinion M_1, M_2, M_3, M_4, M_5 (kg)	1.515
Mass of upper face gear M_6 (kg)	31.295
Mass of lower face gear M_7 (kg)	23.784
Polar inertia of pinion $J_{1z}, J_{2z}, J_{3z}, J_{4z}, J_{5z}$ (kg.m^2)	0.002
Diameter moment of inertia of pinion $J_{1v}, J_{2v}, J_{3v}, J_{4v}, J_{5v}$ ($v = x, y$) (kg.m^2)	0.002
Polar inertia of input shaft J_{1p}, J_{2p} (kg.m^2)	0.0001
Moment of inertia of upper face gear J_{6x}, J_{6y}, J_{6z} (kg.m^2)	0.712, 0.712, 1.407
Moment of inertia of lower face gear J_{7x}, J_{7y}, J_{7z} (kg.m^2)	0.811, 0.811, 1.604
Moment arms of pinion and face gear r_p / r_g (m)	0.039 / 0.243
Backlash of gear pair $2b_{ij}$ ($_i$ =6, 7; $_j$ =1, 2, …5) (m)	20×10^{-6}
Support stiffness of pinion $k_{jx}, k_{j\,y}, k_{jz}$ ($j = 1, 2, …5$) (N/m)	6.5×10^7, 6.5×10^7, 8.5×10^6
Support stiffness of face gear k_{ix}, k_{iy}, k_{iz} (i =6, 7) (N/m)	8.7×10^9, 8.7×10^9, 8.0×10^8
Torsional stiffness of input shaft k_{1t}, k_{2t} (N.m/rad)	6.0×10^5

Table 3 Rated working condition of CFGSTTS

Parameters	Values
Rated input speed n_1, n_2 (rpm)	7600
Rated power of single input P_1, P_2 (kW)	1700
Rated output power of upper face gear P_U (kW)	2500
Rated output power of tail gear P_O (kW)	900
Driving torque of single input T_1, T_2 (N m)	2136
Load torque of upper face gear T_U (N m)	19,530
Load torque of tail gear T_O (N m)	1130

As mentioned in Sect. 2.3.2, the mesh stiffness and TE excitations of the gear pairs in CFGSTTS are time-varying. To improve the numerical accuracy of the dynamic model as much as possible, such time-varying properties should be considered. With reference to the method introduced in Sect. 2.3.1, the mesh stiffness of face gear pairs in CFGSTTS under the working condition in Table 3 is worked out, as demonstrated in Fig. 7.

In Fig. 7, the black dotted line represents the mesh stiffness with standard phase angle, and corresponds to the gear pairs numbered 61, 62, 63, 64 and 75 in Fig. 3. The green solid line means the mesh stiffness with half-period phase angle corresponding to the gear pairs numbered 71, 72, 73, 74 and 65. The average value of the mesh stiffness in Fig. 7 is 4.1178×10^8 N/m, and the harmonic components in Fig. 8 are figured out based on Eq. (1).

TE excitations of gear pairs can be calculated according to the method in Sect. 2.3.2. After the unloaded TE excitation is expanded into Fourier
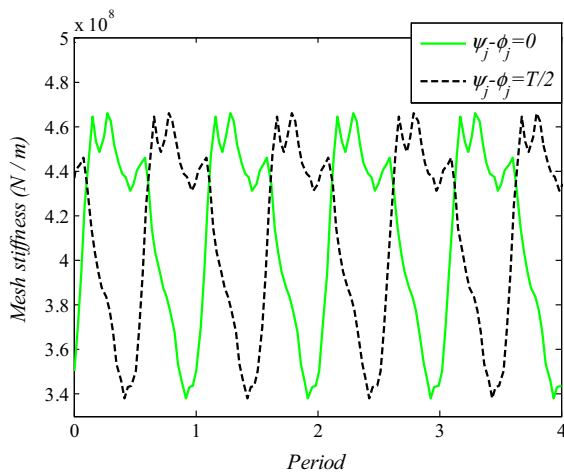
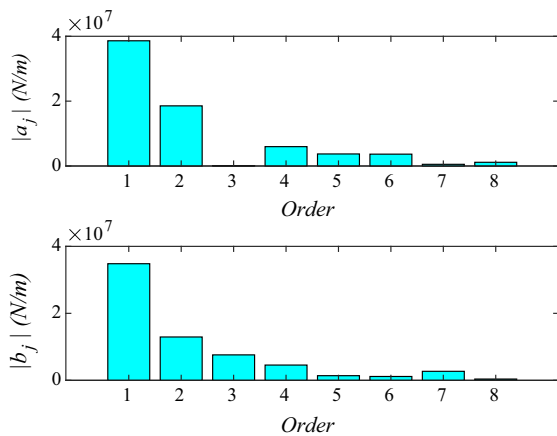**Fig. 7** Time-varying mesh stiffness of face gear pairs in CFGSTTS

Fig. 8 Harmonic components of mesh stiffness

series, all the higher-order components except the 0-order and 1-order harmonic components are filtered out. The TE excitation of the gear pair numbered 61 in Fig. 3 is $e_{61} = e_{m1} + e_{p1}\cos[\omega_m (t - \phi_j + \psi_j)]$. Here, the average e_{m1} is 20×10^{-6} m, and the peak e_{p1} is 25×10^{-6} m. The average and peak of the TE excitations of other gear pairs are coincide with e_{61}, and the phase of the TE excitation is consistent with that of mesh stiffness.

According to Refs. [38–41], the meshing damping c_{ij} ($i = 6, 7$; $j = 1, 2...5$) is formulated as:

$$c_{ij} = 2\zeta_m \sqrt{\frac{k_0}{1/m_p + 1/m_g}} \qquad (22)$$

where ζ_m denotes the mesh damping ratio that is an empirical value, k_0 is the average of time-varying mesh stiffness, and m_w ($w = p, g$) represents the mass of the driving gear and driven gear, respectively. Kahraman et al. [36] and Zhou et al.[39] set a value 0.02 as the meshing damping ratio ζ_m for the spur gear pairs under general meshing conditions, and they stated that the ratio is as large as 0.05 under special working conditions. Omar et al. [40] assumed $\zeta_m = 0.03$ for gear meshing in a spur gearbox. Chen et al. [38] assigned a value 0.045 to ζ_m and obtained the meshing damping $c \approx 1000$ N.s/m in a bevel gear system. Xiao et al. [41] argued that ζ_m usually varied from 0.05 to 0.08. In this paper, ζ_m is assigned as 0.025 for face gear drives, and the symbol m_g is calculated as the average of the mass of two face gears. By substituting $k_0 = 4.1178 \times 10^8$ N/m, $m_p = 1.515$ kg and $m_g = 27.540$ kg into Eq. (22), the meshing damping c is calculated as 1215.9 N.s /m, and the integer value is 1200 N.s /m.

3.1 Natural characteristics

The natural characteristics in modal domain are first analyzed to facilitate the comparison with the responses in time domain later. The natural characteristics of CFGSTTS include natural frequencies, critical speeds and modal shapes, which are determined by the properties of mass and stiffness, rather than backlash or load. The frequency equation is

$$\det\left(K - \omega^2 M\right) = 0 \qquad (23)$$

Here, the symbols K and M are respectively the stiffness matrix and the mass matrix, whose expressions are introduced in Ref. [16]. Besides, the mesh stiffness component in stiffness matrix is substituted by the average value rather than the time-varying stiffness. Based on the parameters in Table 1 and Table 2, the eigenvalues corresponding to 44-order DOFs in Eq. (4) can be directly calculated by using the eigenvalue function command in MATLAB, and the heavy roots should be deleted. Then, the natural frequencies and critical speeds in Table 4 can be obtained correspondingly.

The results in Table 4 indicate that the rated speed in Table 3 (7600 rpm) is distinct from all critical speeds, and the rated speed is between the critical speeds of the 10th and the 11th orders. In addition, the

Table 4 Critical speeds and natural frequencies

Orders (ω_{ith}/n_{ith}) $i = 1, 2\ldots$	Frequencies (Hz)	Speeds (rpm)
0	0	0
1	377.0	983.4
2	745.2	1944.1
3	747.5	1950.0
4	751.3	1959.8
5	756.6	1974.0
6	770.2	2009.3
7	889.5	2320.4
8	1042.5	2719.5
9	1559.8	4069.0
10	2679.5	6990.0
11	3093.8	8070.7
12	3123.9	8149.2
13	5445.1	14,204.6
14	5475.0	14,282.6
15	5508.7	14,370.7
16	5583.0	14,564.3
17	5702.9	14,877.2
18	12,669.3	33,050.3

modal shapes corresponding to the natural frequencies in able 4 are obtained, and one of the modal shapes of each type is selected as the representative, as showed in Fig. 9.

In Fig. 9, the abscissa represents the DOFs in Eq. (4). For instance, the 1th order of abscissa refers to x_1 and the 44th order of abscissa corresponds to θ_{2p}. The ordinate is the ratio of each modal amplitude to the maximum modal amplitude. In general, the modals of CFGSTTS mainly contain translation, torsion, and translation-torsion coupling. Torsion refers to the rotation around the gear axis.

In translational modals, the translation deforms largely and the torsional deformation is close to 0. There are not only single-gear modals, but also some coupled translational modals for multiple pinions. The 1th natural frequency in Table 4 corresponds to the respective translational modals of the five pinions, and Fig. 9a presents the translational modal of left input. The 8th natural frequency in Table 4 corresponds to the coupled translational modal of the five pinons in Fig. 1. In the coupled translational modal illustrated in

Fig. 9b, the modal amplitude of the left pinion is larger than that of the right pinion.

In torsional modals, the torsion deforms largely and the translational deformation is close to 0. The coupled torsional modals consist of multiple gears and input shafts, which correspond to the natural frequencies from 13 to 18th in Table 4. For instance, Fig. 9c illustrates the torsional modal coupled with two input shafts and two input gears, which corresponds to the 18th natural frequency in Table 4. As Fig. 9c shows, the modal deformation of the shaft is significantly greater than that of the gear. Figure 9d shows the torsional modal coupled with two input shafts and five pinions, corresponding to the 17th natural frequency in Table 4. The amplitude of torsional modal of tail gear and two idler gears in Fig. 9d is more obvious than that of two input gears. Besides, the results reveal that input shafts and input gears deform simultaneously in torsional modals.

Additionally, the modals coupled with translation and torsion have the largest number of orders, and the order numbers are from 2 to 7th and from 9 to 12th in Table 4. These coupled modals deform obviously both in translation and torsion. Fig. 9e and Fig. 9f are the translation-torsion modals of seven gears and two input shafts, corresponding to the 13th and 18th natural frequencies in Table 4, respectively. The former involves only translation for face gears, but the latter involves both translation and torsion for face gears. Obviously, the torsional deformation in these coupled modals is larger than the translational deformation.

In conclusion, the high critical speeds (> 10,000 rpm) mainly correspond to torsional modals, while the low critical speeds (< 1500 rpm) and the critical speed 2719.5 rpm in Table 4 mainly correspond to translational modals. Other critical speeds in Table 4 are mainly associated with coupled modals of translation and torsion.

3.2 Dynamic responses and load sharing

According to the parameters in Table 1, Table 2, and Table 3, the time-domain numerical solution of the dynamic equations in Sect. 2.4 can be obtained by using the integration method of Runge–Kutta. According to the authors' statistics, the dynamic equations with single rotation speed and 200 cycles can be solved once every 5 min, and each cycle has 100
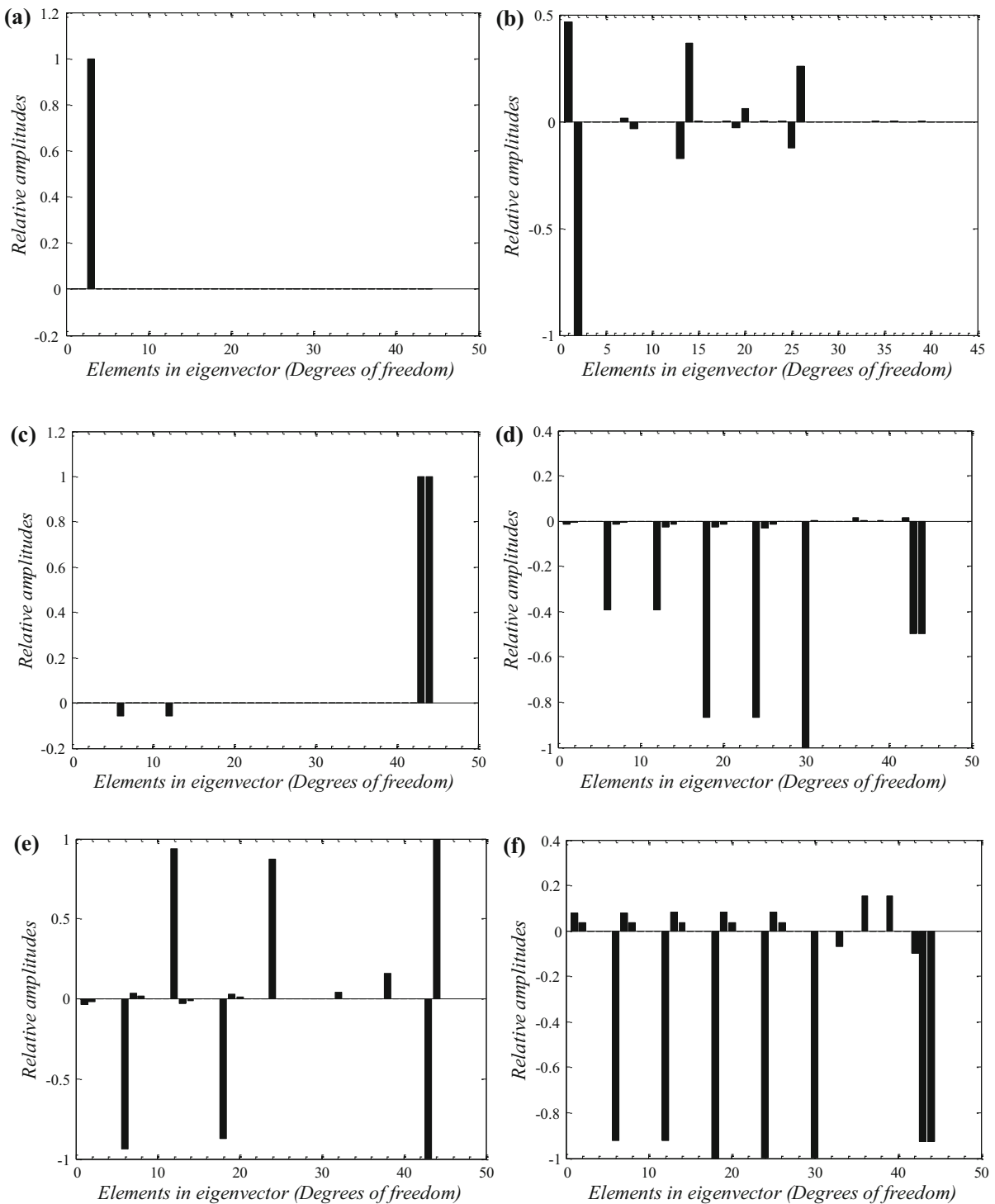
Fig. 9 Modal shapes (**a**) Translation of single pinion (**b**) Translation of pinions (**c**) Torsion of shafts and input gears (**d**) Torsion of shafts and pinions (**e**) Translation-torsion coupling of shafts and gears (**f**) Translation-torsion coupling of shafts and gears

discrete points. According to the responses of 44 DOFs, the DTE and the meshing deformation of each gear pair in CFGSTTS can be figured out, and it is found that the average difference between the former and the latter is within 4%. The DTEs of ten gear pairs are elaborated in Fig. 10, and the torsional angles of two input shafts are presented in Fig. 11.

As presented in Fig. 10, under the rated working condition in Table 3, the DTEs of all gear pairs in CFGSTTS tend to periodic fluctuations. Thus, the system enters into a stable state of vibration. The DTEs of different gear pairs have phase differences, which is determined by the phases of mesh stiffness and TE excitations.

In Fig. 10a and c, the DTEs are fluctuating between 5.0×10^{-5} m and 15.0×10^{-5} m when input gears mesh with upper face gear. The DTEs in Fig. 10b and d are varying between 1.0×10^{-5} m and 8.0×10^{-5} m when input gears mesh with lower face gear. Hence, the excitation of each input gear meshing with upper face gear is greater than that with lower

face gear, because the upper face gear bears a heavy load.

Fig. 10e–h, show that the DTEs of the four gear pairs that are composed of two face gears and two idler gears change from 0 to 4.0×10^{-5} m. Apparently, the vibrations of two idler gears are less than that of two input gears because the idler gears are not driven or loaded directly by torques.

In Fig. 10i, the DTE of the meshing between tail gear and upper face gear fluctuates from -4.0×10^{-5} m to 2.0×10^{-5} m, and the DTE appears the phenomenon of positive and negative signs, which indicates that the contact force and power transmission between the driving gear and the driven gear in this gear pair have changed directions. As demonstrated in Fig. 10j, the DTE of the meshing between tail gear and lower face gear is varying between -3.0×10^{-5} m and -8.0×10^{-5} m. In view of the average value, the DTE of lower face gear is larger than that of upper face gear. The larger average DTEs result from the larger forces. Thus, tail gear is heavily forced by lower face gear, rather than upper
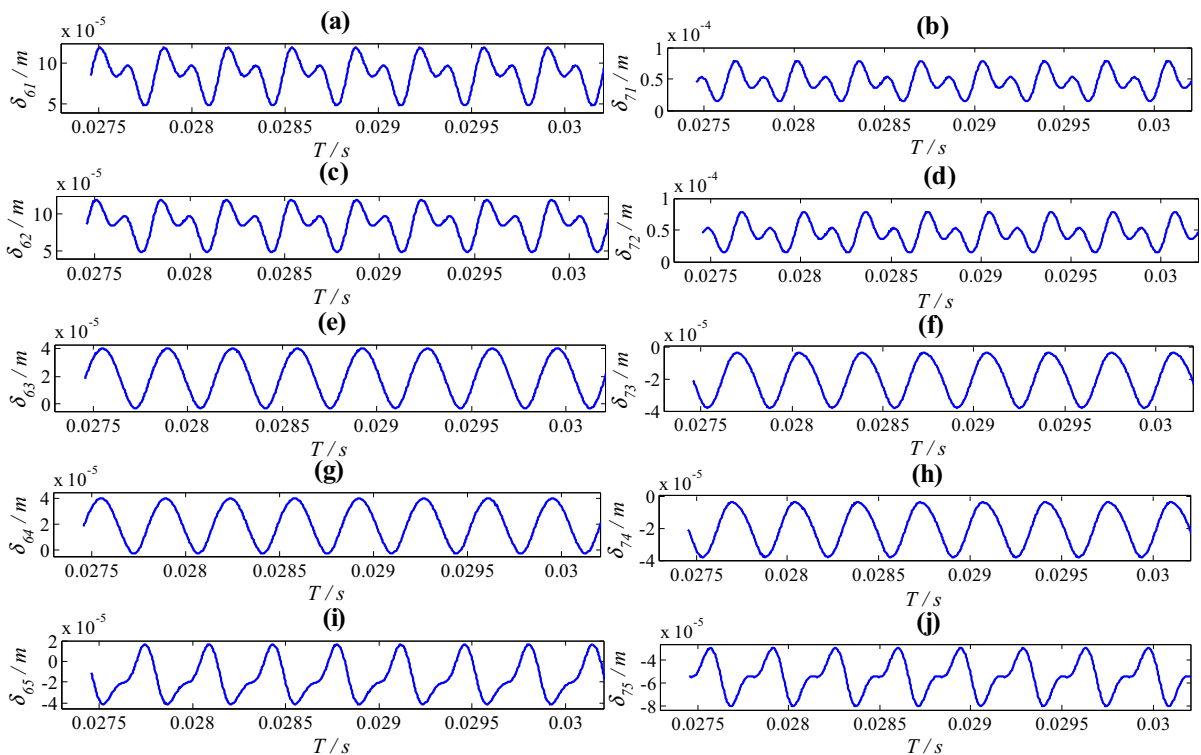

Fig. 10 DTEs of gear pairs (**a**) left input-upper (**b**) left input-lower (**c**) right input-upper (**d**) right input-lower (**e**) left idler-upper (**f**) left idler-lower (**g**) right idler-upper (**h**) right idler-lower (**i**) tail gear-upper (**j**) tail gear-lower
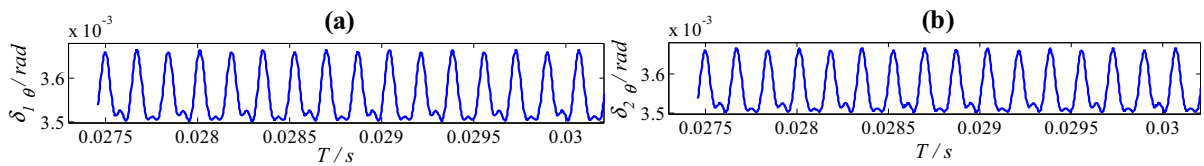
Fig. 11 The angles of torsional deformation of input shafts (**a**) left input shaft (**b**) right input shaft

face gear, which indicates that the vibration of tail gear meshing with lower face gear is greater than that with upper face gear.

In conclusion, the DTEs of all gear pairs in CFGSTTS basically retain at the order of magnitude of 10^{-5} m. Only the DTEs of the meshing between input gears and upper face gear reach the order of magnitude of 10^{-4} m in a short time. The vibrations of input gears are larger than that of idle gears, which reflects the joint excitation effect of driving torques and load torques. Additionally, the vibration of tail gear meshing with upper face gear is less than that with lower face gear, while the other pinions are the opposite, because tail gear has a direct power output.

In Fig. 11, the torsional angles of two input shafts are basically consistent and keep the fluctuations in ranging from 3.5×10^{-3} rad to 3.7×10^{-3} rad. The torsional deformation is affected by the torsional stiffness of input shafts, which will be further studied in the discussion below.

The four-period dynamic contact force of each gear pair in CFGSTTS, as illustrated in Fig. 12, can be calculated by substituting the DTEs in Fig. 10 into Eqs. (8, 9, 11 and 12).

Curves in Fig. 12 denote that the dynamic contact forces are periodic and stable, and their values are the same order of magnitude that is 10^4 N, which preliminarily indicates that the load sharing between gear pairs in CFGSTTS is relatively even. When a pinion simultaneously meshes with two face gears, there is a semi-periodic phase difference between the two contact forces, which is determined by the phase of mesh stiffness.

The peak of the contact force between upper face gear and either of input gears is about 4.8×10^4 N, while the peak of the contact force between lower face gear and either of input gears is about 3.0×10^4 N. Thus, for the same input gear, its contact force stressed by upper face gear is greater than that by lower face gear. Because upper face gear is stimulated by a high-power load torque.

For left idler or right idler, the contact force stressed by upper face gear is equal to that stressed by lower face gear, and the peak force is around 1.3×10^4 N. Both idler gears are not driven or loaded by torques, each idler gear needs to be kept in balance under the action of the contact forces stressed by two face gears. Besides, there is a short period of time in each cycle when the contact force equals 0 N, that is, idler gear separates from meshing with face gears. It is tentatively inferred that this phenomenon may be caused by gear backlash, which will be verified in Sect. 3.3.

There is a big difference between the two contact forces that are generated from tail gear respectively meshing with upper and lower face gears. The peak of contact force generated by upper face gear is about 1.5×10^4 N, and peak of contact force generated by lower face gear is nearly 3.1×10^4 N. Moreover, the contact force between tail gear and upper face gear tends to change direction, which is similar to the result in Fig. 10 (i). Therefore, only part of the power transferred from lower face gear to tail gear is delivered to upper face gear, and the rest of the power is directly output from tail gear.

To sum up, the contact forces of input gears are slightly larger than that of idler gears and tail gear, which is consistent with the conclusions of the static research in Ref. [5]. Particularly, the power transmission direction between tail gear and upper face gear is changing. Based on the method in Ref. [5], the direction of dynamic power flow in CFGSTTS is expressed in Fig. 13.

As the power flow direction in Fig. 13 shows, there are two multi-branch routes for the power transmission in CFGSTTS. One route is that the power of two input gears is directly transferred to upper face gear, and then is to be output. The other route is that the power of input gears is transferred to lower face gear, and then to upper face gear through tail gear and two idler gears, and the tail gear directly output a small amount of power. During a short period of time, there is a reverse
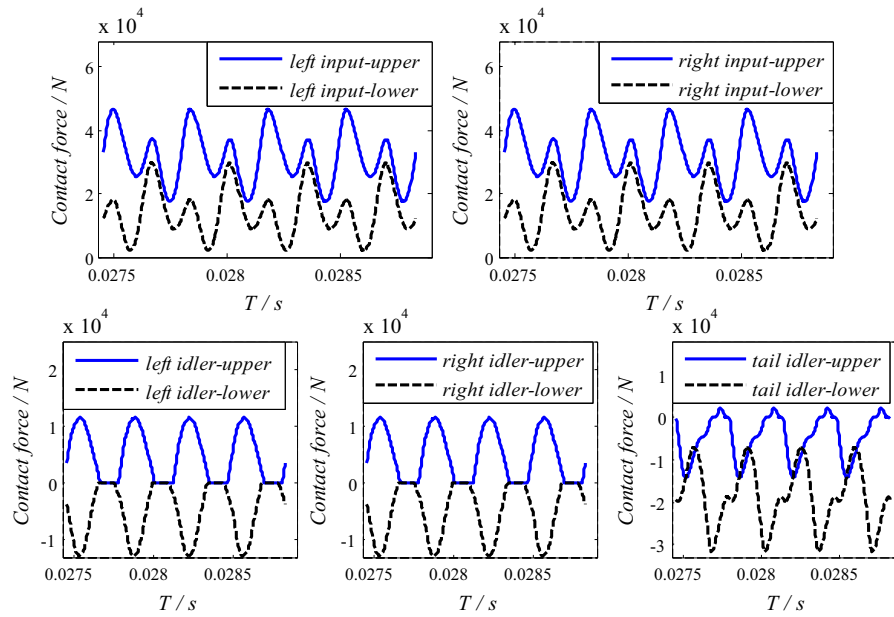
Fig. 12 Four-period dynamic contact forces of gear pairs obtained by LPM
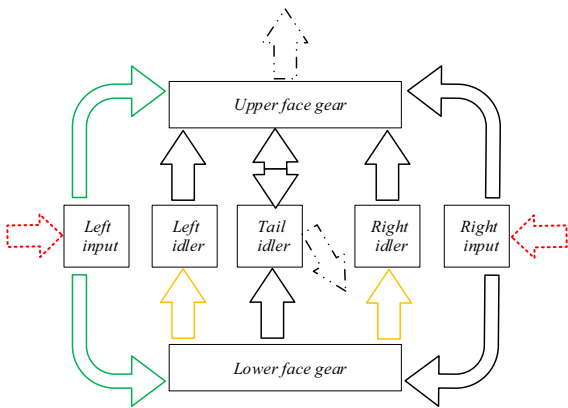

Fig. 13 Dynamic power flow direction of CFGSTTS (red dot arrow: input power; green arrow: power of face gears; orange arrow: power of two idlers)

direction of power flow between tail gear and upper face gear.

To avoid local damages caused by overload, it is necessary to conduct the investigation of dynamic load sharing among different branches. According to the power flow direction in Fig. 13, the CFGSTTS has three cases of load sharing. (i) The load sharing between upper and lower face gears that simultaneously mesh with the same input gear. (ii) The load sharing between two input gears. (iii) The load sharing between left and right idler gears. The cases of load

sharing are basically accordant with static ones in Ref. [5].

According to the definition of LSC in Eq. (21), the dynamic LSCs of CFGSTTS are calculated, as demonstrated in Fig. 14.

According to the curves in Fig. 14, the LSC between two input gears is basically equal to 1.0. It is indicated that the load sharing between two input gears is acceptable.

In the curve of LSC between two idlers, the coefficient also equals 1.0 at most of the periods. However, in a few periods, the LSC has no real value, because the two idlers are not stressed, thus it will not result in the problem of uneven load sharing. It can be concluded that the load sharing between two idlers is relatively ideal.

Additionally, the LSC between two face gears continuously fluctuates from 1.1 to 1.86, and the large values of LSC indicate the poor performance of load sharing. Therefore, the most serious problem of dynamic load sharing is not between two input gears or between two idler gears, but between two face gears during the simultaneously meshing with the same input gear. It can be predicted that damage is most likely to generate in the meshing area between power-input gears and power-output gears in CFGSTTS due to the large stress that exceeds the strength limit. This
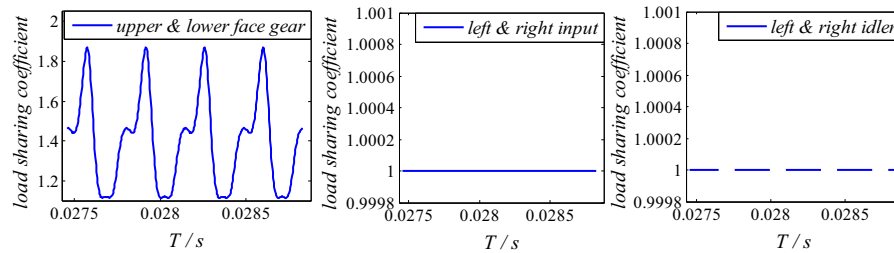
Fig. 14 Dynamic LSCs in four periods

prediction is also applicable to other multi-branch gear systems.

Actually, a gear transmission has to alternatively start and stop, which means that the gears operate at different speeds. In the design stage of a mechanical system, it is necessary to select a rated working condition and set reasonable parameters such as the rated speed. To study the characteristics of dynamic load sharing at different input speeds, 400 speeds are set between 200 rpm and 20,000 rpm for analysis, and the root mean square (RMS) of DTE of gear pairs is figured out, as presented in Fig. 15.

In Fig. 15, the RMS curves of DTEs are fluctuant as the input speed sweeps, and the ten curves change in synchronization. Peaks appear at some special speeds, such as 993 rpm,1986 rpm, 4021 rpm, 7097 rpm and 14,244 rpm. These speeds are nearly close to some critical speeds in Table 4, for instance, 993 rpm $\approx$ n_{1th}, 1986 rpm $\approx n_{5th}$,4021 rpm $\approx n_{9th}$,7097 rpm $\approx n_{10th}$,and 14,244 rpm $\approx n_{14th}$. This phenomenon is resonance.

The extreme points of the ten RMS curves are consistent. However, not all the critical speeds in Table 4 appear extreme values on the RMS curves, which means not all natural frequencies are excited. Even the RMS curves of different DTEs differ slightly in resonance peaks. For instance, when the speed is around 7097 rpm, the resonance peaks are not excited on the four RMS curves δ_{63}, δ_{73}, δ_{64}, and δ_{74}, while the resonance peaks appear on the rest six RMS curves. These four RMS curves correspond to the gear pairs formed by idler gears, which reflects the different dynamic characteristics between idler gears and other pinions.

3.3 Verification

The multi-body simulation in ADAMS software is employed to verify the LPM proposed in this paper. As presented in the dynamic simulation model of CFGSTTS in Fig. 16, the rotation pairs around their axes are established for seven gears, and ten contact pairs are established to simulate the meshing of ten gear pairs that formed by five pinions and two face gears. The time-varying mesh stiffness and the meshing damping coefficient are set according to the parameters in Table 2, the penetration depths of contact pairs are equal to 0.1 mm, and the force exponents are 1.5. By referring to the working condition in Table 3, two input speeds are applied to two input gears, and two load torques are added to upper face gear and tail gear, respectively.

The four-period contact forces of gear pairs in ADAMS model are compared with that of LPM, as illustrated in Fig. 17. Similarly, the LSCs are obtained by adopting the method in Sect. 3.2. Fig. 18 illustrates the comparison diagram of the results of two methods, namely the LPM and the ADAMS model.

As presented in Fig. 17, the contact forces obtained by the ADAMS model are basically consistent with those gained by the LPM in both the size and the variation trend. In view of the average value, the contact force of the meshing between left input and upper face gear in ADAMS model is 3.47×10^4 N, and the contact force of the same gear pair in LPM is 3.13×10^4 N. The difference between the two average values is 9.8%. Besides, the differences between the contact forces of other gear pairs calculated with the two models are within 9.8%.

At 0.0278 s, the contact forces between tail gear and two face gears in LPM appear abrupt peaks. The authors believe that this situation is related to the sensitivity of the initial value near 0 in the iterative
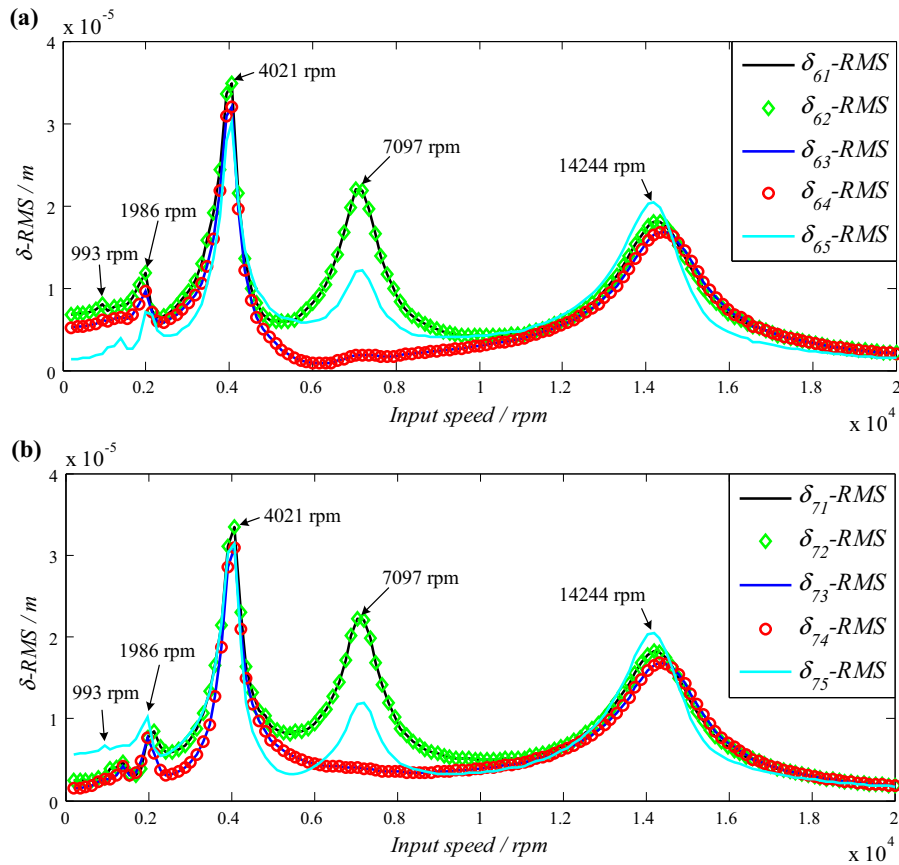
Fig. 15 RMS curves of DTEs of gear meshing (**a**) Gear pairs formed by upper face gear (**b**) Gear pairs formed by lower face gear
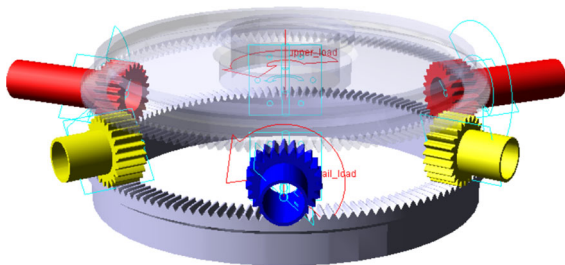

Fig. 16 Dynamic simulation model in ADAMS (red arrow: load torques; light blue arrow: input speeds; light blue rectangle: rotation pairs)

algorithm. Since the contact force is about 0, these peaks can be filtered out.

At 0.0278 s, the contact forces of left and right idlers in ADAMS model appear non-zero values earlier than that in LPM, which is caused by the errors of the geometric model imported into ADAMS software. The geometric surfaces of face gears are obtained by fitting with the discrete points calculated by the face gear equations. In the ADAMS simulation of the gear transmission with high speed, the pinion without driving torque or load torque is more sensitive to small geometric errors.

In Fig. 18, the curve variation trend of the LSCs calculated by two methods is basically identical. The average values of the LSCs of two face gears obtained by using two models are 1.4428 and 1.3982, which companies with a difference of 3.1%. The averages of the LSCs of two input gears are respectively 1.0099 and 1.0, which companies with a difference of 0.99%.

In the LSC curves of two idler gears, there is a special period in which the LSC is either equal to 2 or invalid, because the forces on two idlers are close to 0 during this special period (see Fig. 17). In Fig. 18, the LSCs in addition to the special period are basically kept within 1.2. There is no statistical value of the LSCs in the special period, which should be ignored.
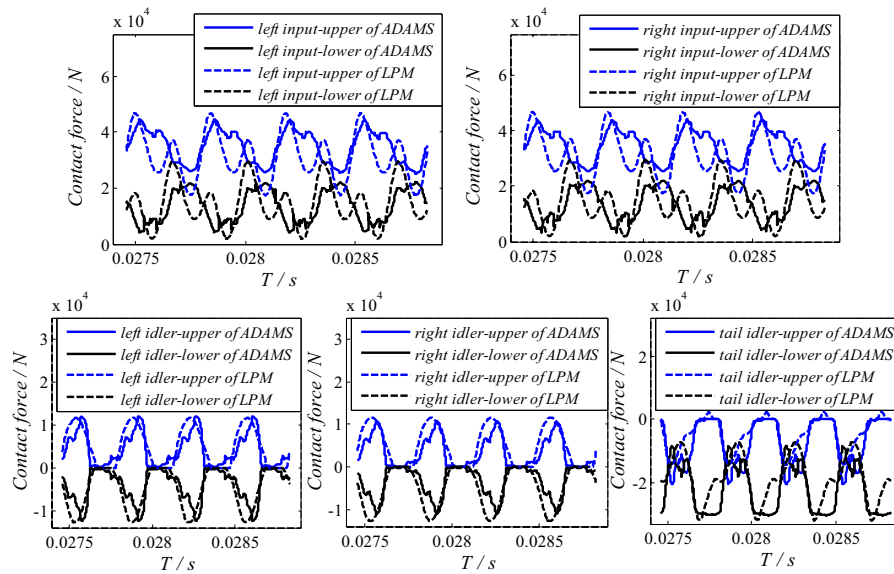
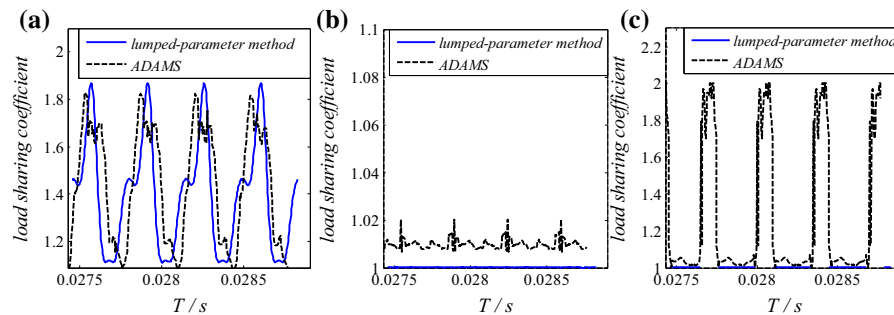Fig. 17 Comparison of ADAMS model and LPM

Fig. 18 Comparison diagram of LSCs with two methods (**a**) two face gears (**b**) two input gears (**c**) two idlers

Therefore, the averages of the LSCs of two idlers are 1.035 and 1.0 respectively, and the difference is 3.5%.

In conclusion, the differences of both the contact forces and LSCs obtained by the two models are acceptable, which has verified the calculating accuracy of the proposed LPM. However, in both Fig. 17 and Fig. 18, the curves extracted from the ADAMS simulation are smooth, while the curves figured by LPM have burrs. The main reason of the differences are the precision deficiencies of the multi-body dynamic model in ADAMS. For instance, the penetration depth is not an accurate value, but is selected according to the meshing deformation. In addition, the force exponent in ADAMS model is selected according to experience.

Furthermore, to verify the conclusion in Sect. 3.2 that gear backlash may cause the tooth disengagement of idler gears, the LSCs of the system without backlash are also calculated, as demonstrated in Fig. 19.

In Fig. 19, all points in LSC curves without backlash have continuous effective values, and the LSC equal to 2.0 is not obtained. According to the definition of LSC in Eq. (21), there is no case that gears are not stressed, which means the disappearance of the tooth disengagement in Fig. 12. Therefore, gear backlash is one of the causes of the disengagement of two idler gears.
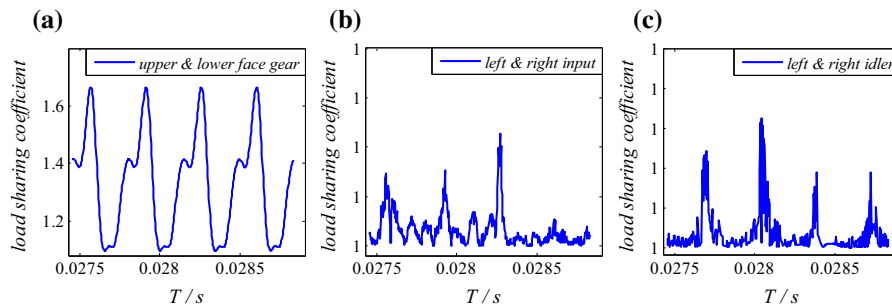
Fig. 19 LSCs without backlash (**a**) two face gears (**b**) two input gears (**c**) two idlers

4 Discussions

In fact, it is difficult to make the service life of different gear pairs in CFGSTTS to become the same. Thus, appropriate structural parameters should be designed to make the load sharing as even as possible.

As concluded in Sect. 3.2, the load sharing between two input gears and that between two idler gears are reasonable and acceptable. However, poor performance of load sharing occurs when two face gears mesh with the same input gear. Therefore, this section focuses on the influence of system parameters on the dynamic load sharing between two face gears in CFGSTTS.

Without the special explanation, the geometric parameters of CFGSTTS in all examples of this section are presented in Table 1. The parameters of the dynamic model are in Table 2 and the parameters used for the load working condition are presented in Table 3.

4.1 Effect of gear backlash on dynamic load sharing

The current research [36] indicated that gear backlash has a great influence on the dynamic responses of gear transmissions. As mentioned above, the functions of the pinions in CFGSTTS are different, though these pinions have same tooth surface parameters. In practical application, the backlash value of gear pairs can be differently controlled.

To respectively study the effect of the backlash of input gears, idler gears and tail gear on the dynamic performance of CFGSTTS, the following comparative analyses are made. (i) All gear pairs have no backlash. (ii) The backlash values 2b of the gear pairs that contain input gears are 20 um, and the rest gear pairs

have no backlash. (iii) The backlash values 2b of the gear pairs that contain idler gears are 20 um, and the rest gear pairs have no backlash. (iv) The backlash values 2b of the gear pairs that consist of tail gear are 20 um, and the rest gear pairs have no backlash. (v) All gear pairs have the same gear backlash with the value of 20 um. LSCs in above-mentioned five cases were compared in a single period, as demonstrated in Fig. 20.

In Fig. 20, the LSC curve in case (ii) is basically coincident with that in case (v). In these two cases, gear backlash appears in the gear pair containing input gear, or in all gear pairs. Likewise, the LSC curve in case (i) is coincident with those in case (iii) and case (iv). The characteristics of these three cases are that the backlash values of the gear pairs containing input gears are 0 um.

During the period from 0.02755 s to 0.0276 s, there is no backlash for input gears when the peaks of LSC are 1.68 in cases (i), (iii) and (iv). The backlash of
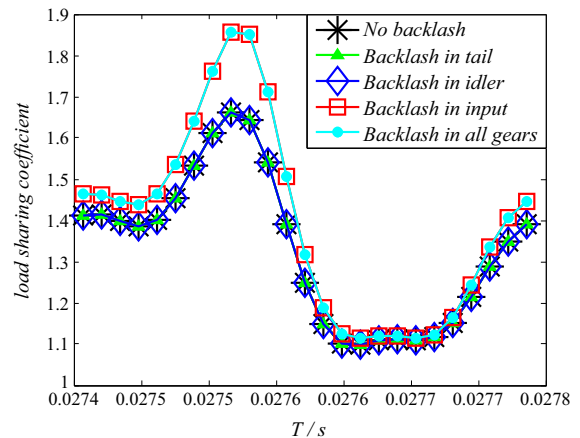

Fig. 20 Effect of different pinion backlash on dynamic load sharing

input gears is not equal to 0 um when the LSC peaks reach 1.86 in cases (ii) and (v). As a result, the value of LSC trends to be smaller if the input gear has no backlash.

These analytical results fully show that the backlash of input gears has the most significant effect on the dynamic responses of CFGSTTS. The backlash of the gear pairs that are not composed of input gears has less effect on the dynamic performance.

Actually, it is high precision for gear pairs if the value of backlash 2b is equal to 20 um. The single-period LSC curves in Fig. 21 corresponds to the situation that all gear pairs in CFGSTTS have same backlash.

During the period from 0.0275 s to 0.0276 s, when the backlash value 2b is 0 um or 20 um, the corresponding peaks of LSC are 1.65 or 1.88 respectively. While the gear backlash is greater than or equal to 40 um, the peak of LSC in this period reaches 2.0, that is, tooth disengagement occurs.

Similarly, during the period from 0.0277 s to 0.0278 s, as the backlash value 2b increases successively from 0 to 80 um, the peak of LSC increases from 1.40 to 2.0.

It can be concluded from the results in Fig. 21 that when the backlash value increases, the whole LSC will become larger. That means gear backlash is unfavorable to the performance of dynamic load sharing in CFGSTTS. It is suggested that backlash design should consider the current manufacturing technology and

minimize the backlash value without affecting the assembly. For the consistency of gear manufacturing process, the gear backlash of all gear pairs should be set the same value.

4.2 Effect of torsional stiffness of input shafts on dynamic load sharing

A highlight of the dynamic model in this paper is the consideration of the torsional deformation of input shafts. In the research of static simulations, it was proved that the flexibility of input shafts has a certain effect on the characteristics of static load sharing in CFGSTTS. Therefore, it is necessary to explore whether the torsional stiffness of input shafts has effect on dynamic load sharing of CFGSTTS. Different values are set for the torsional stiffness k_{ti} ($i = 1, 2$) of input shafts, and the comparative curves of single-period LSC are presented in Fig. 22.

In Fig. 22, the LSC differs as the value of torsional stiffness changes, which indicates the torsional stiffness of input shafts has significant effect on dynamic load sharing.

In the period of 0.0275 s to 0.0276 s, the peak of LSC is 2.0 when the value of torsional stiffness is 6.0×10^4 N.m/rad, which means that there has been the tooth disengagement. While the values of torsional stiffness are equal to 6.0×10^3 N.m/rad, 6.0×10^5 N.m/rad, 6.0×10^6 N.m/rad and 6.0×10^7 N.m/rad, respectively, the corresponding
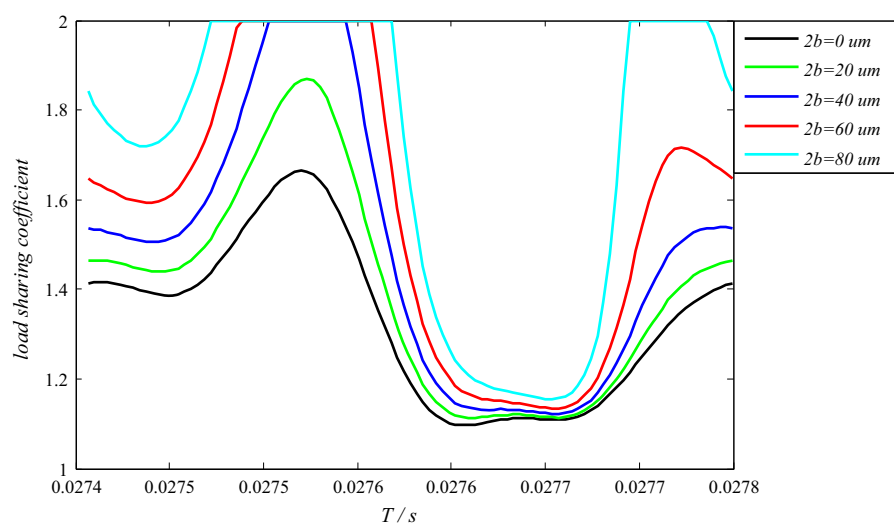

Fig. 21 Dynamic LSCs with different backlash values
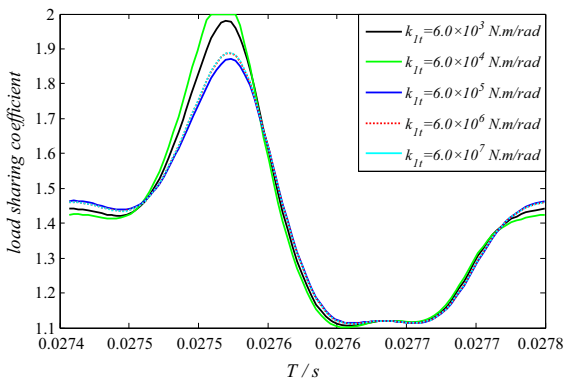
Fig. 22 Effect of the torsional stiffness of input shafts on dynamic load sharing

peaks of LSC are 1.98, 1.85, 1.87 and 1.87. Thus, as the torsional stiffness increasingly grows, the corresponding LSC tends to decrease and then increase, and the phenomenon of tooth disengagement starts from being to not being. In other periods, the LSCs of five different torsional stiffness are close.

Therefore, the torsional stiffness of input shafts has great effect on the characteristics of dynamic load sharing in CFGSTTS, but this effect is not positive correlation. There is an optimal range of torsional stiffness, which corresponds to the smallest LSC and the best performance of load sharing. Some larger or smaller values are not conducive to the dynamic load sharing. In this example, an optimal range of the torsional stiffness is around 6.0×10^5 N.m/rad.

4.3 Effect of time-varying mesh stiffness on dynamic load sharing

The mesh stiffness in Fig. 7 is calculated based on a specific material and load condition, and the mesh stiffness can be redesigned by changing the gear material and operating conditions. Thus, it is significant to research the effect of mesh stiffness on dynamic load sharing of CFGSTTS. The single-period LSCs corresponding to the mesh stiffness with the same phase as Sect. 3 and different averages are demonstrated in Fig. 23.

The phase is another variable of the time-varying mesh stiffness in addition to the average. According to the static research in Ref. [6], when the tooth number of a pinion is odd, there must be a half-period phase difference in the mesh stiffness of two gear pairs formed by the same pinion. However, when the number of teeth is even, the phase difference disappears. The comparative diagram of the dynamic LSCs corresponding to two kinds of phases are presented in Fig. 24.

Obviously, the dynamic LSCs in Fig. 23 vary greatly as the averages of mesh stiffness change. As the average of mesh stiffness gradually increases from 9.0×10^7 N/m to 8.0×10^8 N/m, the corresponding LSC increases from 1.70 to 1.9 during the period of 0.0275 s to 0.0276 s, but dramatically decreases from 1.90 to 1.42 during the period of 0.0277 s to 0.0278 s. The tendencies in these two periods are opposite. The LSC curve is relatively flat when the average of mesh stiffness is 2.0×10^8 N/m. Therefore, the average of mesh stiffness also has ideal values, which makes the dynamic load sharing performance optimal. The values of mesh stiffness greater or less than the ideal values are not conducive to the performance of dynamic load sharing. One of the ideal values in this example is about 2.0×10^8 N/m.

In Fig. 24 the LSC changes markedly as the mesh stiffness phase differs. In the period of 0.0275 s to 0.0276 s, the peak of LSC is 1.90 when the tooth number is odd. However, the peak of LSC is 1.40 when the tooth number is even. The difference of the peaks of LSC in the two cases is 26.3%. During the period from 0.0277 s to 0.0278 s, the peak of LSC is 1.42 for the case of odd tooth number, and the peak of LSC is 2.0 for the case of even tooth number. Thus, the phase difference to a great degree affect the performance of dynamic load sharing. Moreover, the pinion with odd tooth number can achieve the better performance of dynamic load sharing in CFGSTTS than that of even tooth number, which explains why the tooth number of the pinion in Table 1 is 23.

5 Conclusions

A LPM with 44 DOFs is proposed to explore the torsional vibrations of input shafts, the meshing vibrations, as well as the translational, torsional, and bending vibrations of gears in CFGSTTS. The TE formulation adopted in the dynamic model is modified according to the characteristics of face gear drives. Through analyzing the dynamic simulation results of ADAMS, the accuracy of the proposed model is identified to be acceptable.
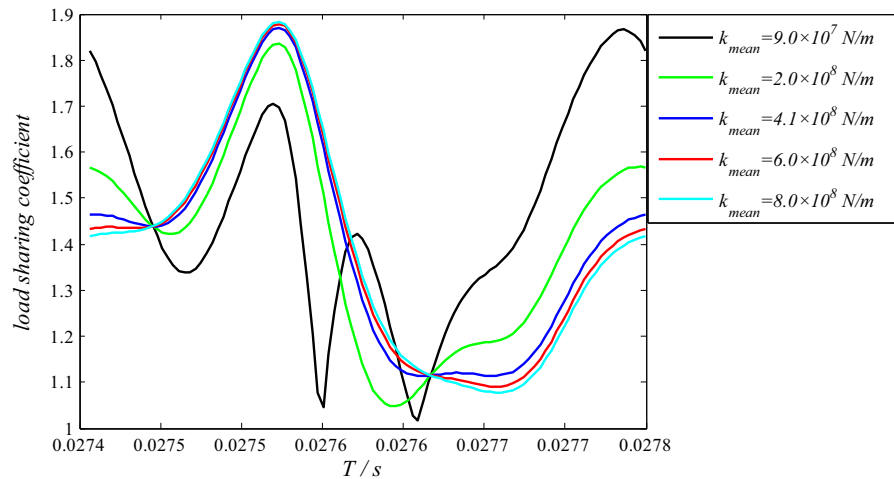
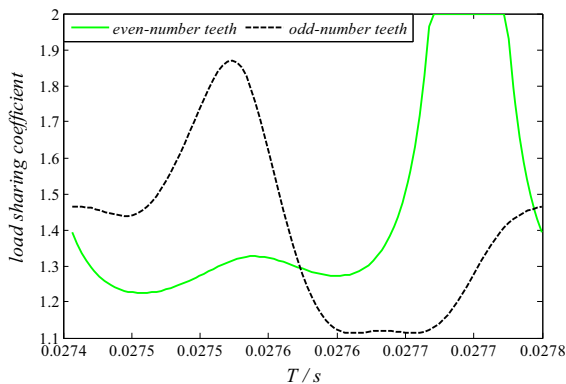**Fig. 23** Effect of the average of mesh stiffness on dynamic load sharing

Fig. 24 Effect of mesh stiffness phases on dynamic load sharing

The natural characteristics of CFGSTTS such as critical speeds and modal shapes are presented. The rated speed 7600 rpm differs from all critical speeds, and the modal shapes of the system mainly are translation, bending, torsion, and translation-torsion coupling.

The dynamic response and load sharing under a rated condition is researched, in which the phenomenon of tooth disengagement is observed in a short period. The research show that the dynamic loads between two input gears and that between two idler gears are shared more even than that between two face gears. The vibrations of input gears are more violent than that of idler gears. The vibration of tail gear in the engagement with upper face gear is more moderate than that with lower face gear, while other pinions is

the opposite. In addition, the speed-sweep response is studied and compared with the critical speeds, and resonances would occur at partial critical speeds.

The factors including the torsional stiffness of input shafts, the time-varying mesh stiffness, and the gear backlash affect the performance of dynamic load sharing in CFGSTTS. Through utilizing the verified dynamic model to investigate these effects, the following conclusions are drawn. (i) The backlash of the gear pairs of the input gears has a tremendous effect on the system. In a certain range, the gear backlash should be controlled as small as possible, which is beneficial to the dynamic load sharing. (ii) Both the torsional stiffness of input shafts and the time-varying mesh stiffness of gear pairs have optimal values, which can achieve the advantageous performance of dynamic load sharing, while the larger or smaller stiffness values need to be avoided. (iii) The phase of mesh stiffness also has a significant influence on dynamic load sharing, and the phase difference of mesh stiffness between different gear pairs is favorable to dynamic load sharing.

Declarations

Conflict of interest The authors declare that they have no conflict of interests.

References

1. Litvin FL, Wang JC (1992) Face-gear drives: design, analysis, and testing for helicopter transmission applications. NASA Tech Memo 106101
2. Litvin FL, Wang JC, Bossler RB, Chen YJD, Heath G, Lewicki DG (1994) Application of face-gear drives in helicopter transmissions. J Mech Des 116(3):672–676
3. White G (1998) Design study of a split-torque helicopter transmission. Proc Instn Mech Eng Part G J Aero Eng 212(G2):117–123
4. Krantz TL, Delgado IR (1996) Experimental study of split-path transmission load sharing. NASA Tech Memo 107202
5. Dong J, Tang J, Hu Z (2019) Investigation of assembly, power direction and load sharing in concentric face gear split-torque transmission system. Mecca 54(15):2485–2506
6. Dong J, Tang J, Hu Z, Wang Y (2020) A semi-analytical method of time-varying mesh stiffness in concentric face gear split-torque transmission system. J Mech Scie Tech 34(2):589–602
7. Litvin FL, Fuentes A, Zanzi C, Pontiggia M (2002) Design, generation, and stress analysis of two versions of geometry of face-gear drives. Mech Mach Theory 37(10):1179–1211
8. Litvin FL, Fuentes A, Zanzi C (2002) Face-gear drive with spur involute pinion: geometry, generation by a worm, stress analysis. Comput Methods Appl Mech Engrg 191(25–26):2785–2813
9. Litvin FL, Gonzalez-Perez I, Fuentes A, Vecchiato D, Hansen BD, Binney D (2005) Design, generation and stress analysis of face-gear drive with helical pinion. Comput Methods Appl Mech Engrg 194(36–38):3870–3901
10. Litvin FL (1994) Gear geometry and applied theory. PTR Prentice Hall, USA
11. Zhou Y, Wu Y, Wang L, Tang J, Ouyang H (2019) A new closed-form calculation of envelope surface for modeling face gears. Mech Mach Theory 137:211–226
12. Zschippang HA, Weikert S, Küçük KA, Wegener K (2019) Face-gear drive: geometry generation and tooth contact analysis. Mech Mach Theory 142:1–37
13. Liu D, Ren T, Jin X (2015) Geometrical model and tooth analysis of undulating face gear. Mech Mach Theory 86:140–155
14. Shen Y, Liu X, Li D, Li Z (2018) A method for grinding face gear of double crowned tooth geometry on a multi-axis CNC machine. Mech Mach Theory 121:460–474
15. Handschuh RF, D.g. Lewicki, R.B. Bossler, (1994) Experimental testing of prototype face gears for helicopter transmissions. Proc Instn Mech Eng Part G J Aero Eng 208(G2):129–136
16. Hu Z, Tang J, Chen S, Sheng Z (2015) Coupled translation-rotation vibration and dynamic analysis of face geared rotor system. J Sound Vib 351:282–298
17. Hu Z, Tang J, Chen S, Cai D (2013) Effect of mesh stiffness on the dynamic response of face gear transmission system. J Mech Des 135(7):1–7
18. Lin C, Liu Y, Gu S (2015) Analysis of nonlinear twisting vibration characteristics of orthogonal curve-face gear drive. J Braz Soc Mech Sci Eng 37:1499–1505
19. Lin C, Cai Z (2016) Modeling of dynamic efficiency of curve-face gear pairs. Proc IMechE Part C J Mech Engr Sci 230(7–8):1209–1221
20. Li Z, Liu S, Zhu R, Xu X (2016) Investigations of dynamic behaviors of face gear drives associated with pinion dedendum fatigue cracks. Shock Vib 2016:1–10
21. Li Z, Wang H, Zhu R (2019) Effect predictions of web active control on dynamic behaviors of face gear drives. J Low Freq Noise Vib Active Cont 38(2):753–764
22. Chen S, Tang J, Chen W, Hu Z, Cao M (2014) Nonlinear dynamic characteristic of a face gear drive with effect of modification. Mecca 49(5):1023–1037
23. Liu D, Gu D, Liu Z (2019) Coupled vibration modeling and dynamic characteristics of noncircular face gear drive system with time-varying instantaneous center excitation. Proc IMechE Part C J Mech Eng Sci 233(14):4947–4959
24. Zhu L, Shi J, Gou X (2020) Modeling and dynamics analyzing of a torsional-bending-pendular face-gear drive system considering multi-state engagements. Mech Mach Theory 149:103790
25. Hu Q, Chen X, Xu Z, Mai Q, Zhu C (2020) Study on kinematic characteristics of planetary multistage face gears transmission. Proc IMechE Part D J Auto Eng 234(2–3):572–585
26. Chen X, Hu Q, Xu Z, Zhu C (2019) Numerical modeling and dynamic characteristics study of coupling vibration of multistage face gears planetary transmission. Mech Scie 10:475–495
27. Singh A (2005) Application of a system level model to study the planetary load sharing behavior. J Mech Des 127(3):469–476
28. Singh A, Kahraman A, Ligata H (2008) Internal gear strains and load sharing in planetary transmissions: model and experiments. J Mech Des 130:072602
29. Ligata H, Kahraman A, Singh A (2009) A closed-form planet load sharing formulation for planetary gear sets using a translational analogy. J Mech Des 131(2):021007
30. Montestruc AN (2010) A numerical approach to calculation of load sharing in planetary gear drives. J Mech Des 132(1):014503
31. Montestruc AN (2011) Influence of planet pin stiffness on load sharing in planetary gear drives. J Mech Des 133(1):014501
32. Iglesias M, Rincon AF, A. de-Juan, P. Garcia, A. Diez-Ibarbia, F. Viadero, (2017) Planetary transmission load sharing: manufacturing errors and system configuration study. Mech Mach Theory 111:21–38
33. Li M, Xie L, Ding L (2017) Load sharing analysis and reliability prediction for planetary gear train of helicopter. Mech Mach Theory 115:97–113
34. Mo S, Zhang T, Jin G, Cao X, Gao H (2020) Analytical investigation on load sharing characteristics of herringbone planetary gear train with flexible support and floating sun gear. Mech Mach Theory 144:103670

35. Mo S, Yue Z, Feng Z, Shi L, Zou Z, Dang H (2019) Analytical investigation on load-sharing characteristics for multi-power face gear split flow system, Proc IMechE Part C. J Mech Engrg Scie 54(15):2485–2506
36. Kahraman A, Singh R (1990) Non-linear dynamics of a spur gear pair. J Sound Vib 142(1):49–75
37. Xiang D, Shen Y, Wei Y (2019) A contact force model considering meshing and collision states for dynamic analysis in helical gear system. Chin J Mech Eng 32(1):32–41
38. Chen W, Chen S, Hu Z, Tang J, Li H (2020) Dynamic analysis of a bevel gear system equipped with finite length squeeze film dampers for passive vibration control. Mech Mach Theory 147:103779

39. Zhou S, Song G, Sun M, Ren Z (2018) Nonlinear dynamic response analysis on gear-rotor-bearing transmission system. J Vib Control 24:1632–1651
40. Omar FK, Moustafa KA, Emam S (2012) Mathematical modeling of gearbox including defects with experimental verification. J Vib Control 18:1310–1321
41. Xiao Z, Zhou C, Chen S, Li Z (2019) Effects of oil film stiffness and damping on spur gear dynamics. Nonlinear Dyn 96:145–159